On Electron Heating, Deposition Rate, and Ion Recycling in the High Power Impulse Magnetron Sputtering Discharge

Jón Tómas Guðmundsson[1,2]

[1] Science Institute, University of Iceland, Reykjavik, Iceland
[2]Division of Space and Plasma Physics, KTH Royal Institute of Technology, Stockholm, Sweden

ISPlasma2023/IC-PLANTS2023
Gifu University, Gifu Japan
March 5., 2023

Introduction – Magnetron sputtering

- Physical vapor deposition (PVD) refers to the removal of atoms from a solid or a liquid by physical means, followed by deposition of those atoms to form a thin film or coating

Gudmundsson et al. (2022) PSST **31** 083001

- Sputtering, which is dominated by magnetron sputtering, is the most widely used such technique

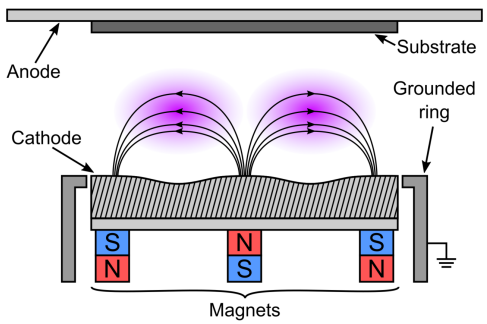

Gudmundsson and Lundin (2020) in High Power Impulse Magnetron Sputtering Discharge, Elsevier, 2020

- Magnetron sputtering has been a highly sucessfull technique that is essential in a number of industrial applications

Introduction – Magnetron sputtering

- A magnetron sputtering discharge is a magnetically enhanced diode sputter tool, based on magnetically trapping electrons in the cathode vicinity

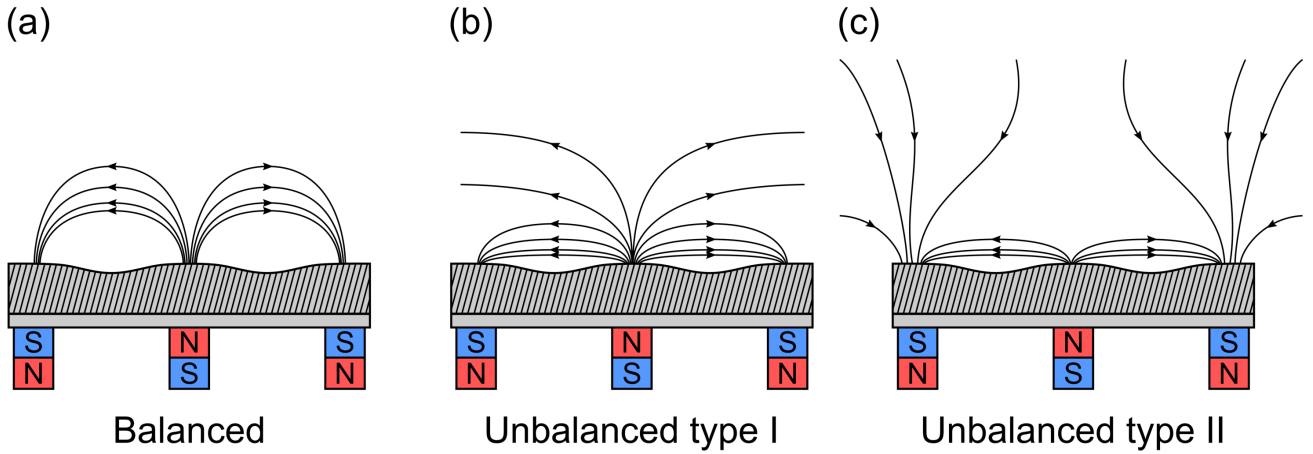

Gudmundsson and Lundin (2020) in High Power Impulse Magnetron Sputtering Discharge, Elsevier, 2020

- Magnets are placed at the back of the cathode target with the pole pieces at the center and perimeter
- The electrons undergo numerous ionizing collisions before being lost to a grounded surface

Introduction – Magnetron sputtering

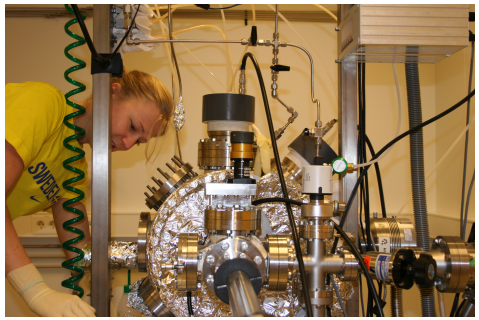

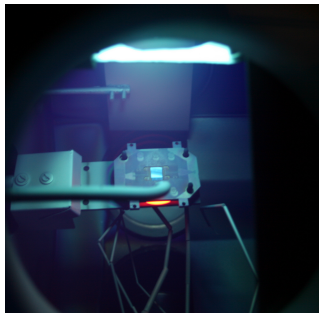

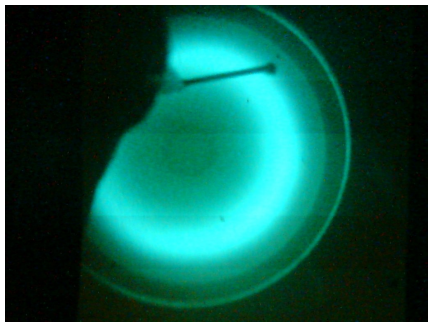

- Magnetron sputtering has been the workhorse of plasma based sputtering methods for almost five decades
- Through the years there has been a continuous development of the magnetron sputtering processes to
  - increase the ionization of the sputtered vapor
  - improve target utilization
  - avoid target poisoning in reactive sputtering
  - increase deposition rates

Introduction – Magnetron sputtering

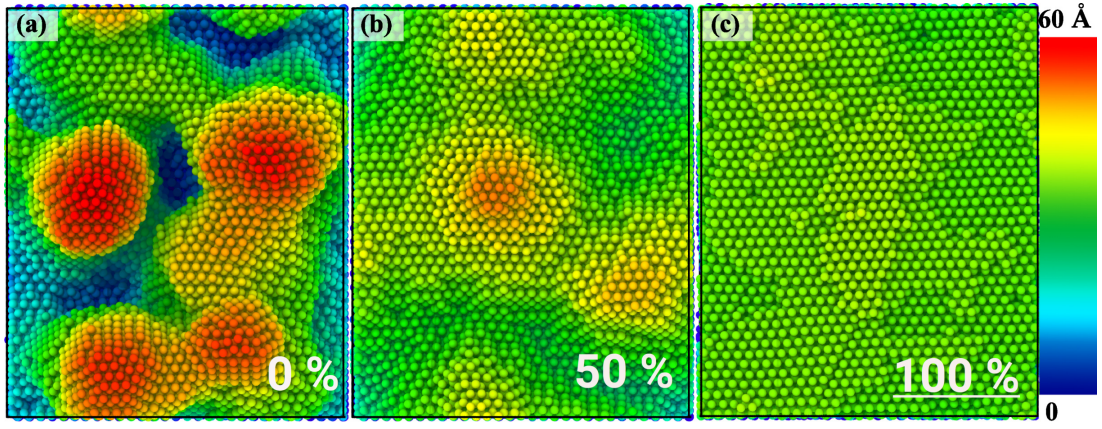

Kateb et al. (2019) JVSTA **37** 031306

- For many applications a high degree of ionization of the sputtered vapor is desired
  - controlled ion bombardment of the growing film
  - ion energy – can be controlled by a negative bias applied to the substrate
  - collimation – enhanced step coverage
- Ionized flux of the sputtered material introduces an additional control parameter into the deposition process

Introduction – magnetron sputtering

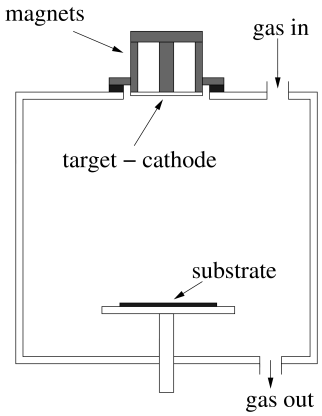

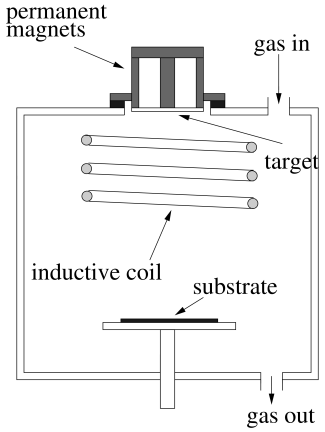

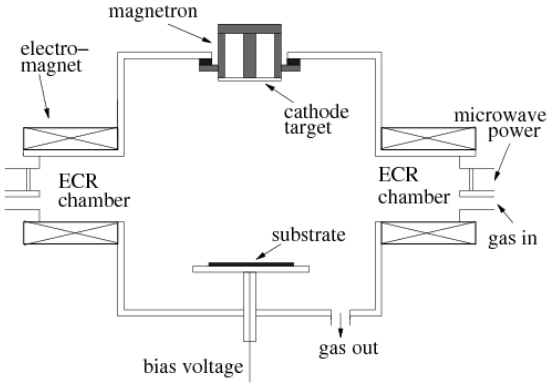

From Gudmundsson (2008), J. Phys.: Conf. Ser. **100** 082002

- In magnetron sputtering discharges increased ionized flux fraction is achieved by
  - a secondary discharge between the target and the substrate (rf coil or microwaves)
  - reshaping the geometry of the cathode to get more focused plasma (hollow cathode)
  - increasing the power to the cathode (high power pulse)
- Common to all highly ionized magnetron sputtering techniques is a very high density plasma

Overview

- The high power impulse magnetron sputtering discharge (HiPIMS)
- Thin film deposition
- The ionization region model (IRM)
- Working gas rarefaction
- Electron power absorption
- Deposition rate vs ionized flux fraction
- Recycling in HiPIMS discharges
- Summary

The high power impulse magnetron sputtering discharge (HiPIMS)

High power impulse magnetron sputtering discharge

- In a dc magnetron sputtering discharge the power density is limited by the thermal load on the target
- Most of the ion bombarding energy is transformed into heat at the target
- In a HiPIMS discharge a high power pulse is supplied for a short period
  - low frequency
  - low duty cycle
  - low average power
- The high power pulsed magnetron sputtering discharge uses the same sputtering apparatus except the power supply

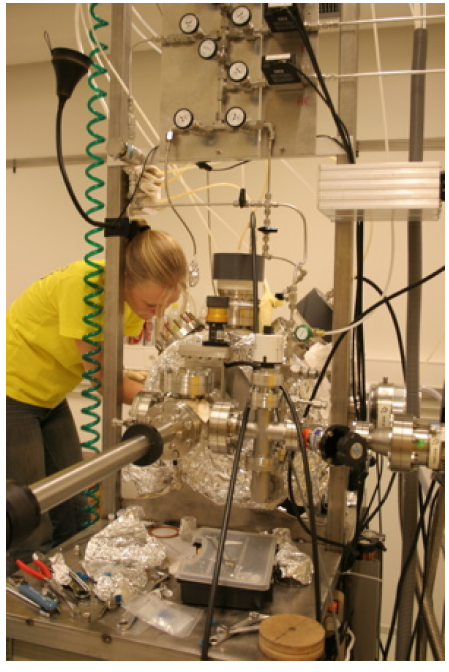

High power impulse magnetron sputtering discharge

- To keep the thermal load below the target damage limit the power density can be increased as the duty cycle is shortened
- High power pulsed magnetron sputtering (HPPMS)
- High power impulse magnetron sputtering (HiPIMS)
  - a pulse of very high amplitude, an impulse, is applied to the cathode and a long pause exists between the pulses
- Modulated pulse power (MPP)
  - the initial stages of the pulse (few hundred μs) the power level is moderate (typical for a dcMS) followed by a high power pulse (few hundred μs up to a ms)

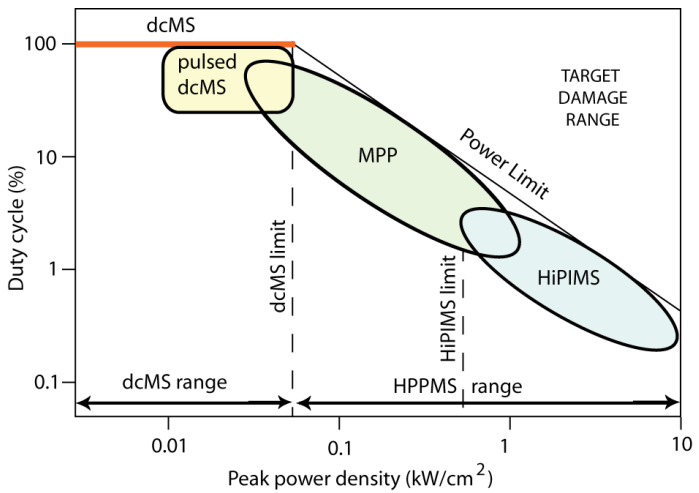

Gudmundsson et al. (2012) JVSTA **30** 030801

- Power density limits
  $p_t = 0.05$ kW/cm^2 dcMS limit
  $p_t = 0.5$ kW/cm^2 HiPIMS limit

Thin film deposition

Thin film deposition

- In HiPIMS deposition, the high fraction of ionization of the sputtered species has been shown to lead to
  - the growth of smooth and dense films
  - enable control over their phase composition and microstructure
  - enhance mechanical and optical properties
  - improving film adhesion
  - enabling deposition of uniform films on complex-shaped substrates
- For optimization of HiPIMS thin film deposition processes, quantification and control of the fraction of ionization of the sputtered species are for obvious reasons key requirements

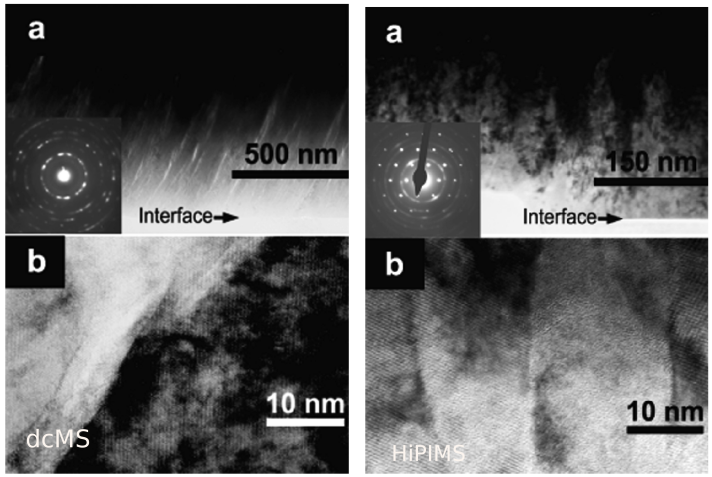

dc magnetron HiPIMS

After Alami et al. (2005) JVSTA, **23** 278

Thin film deposition

- The film mass density is always higher when depositing with HiPIMS compared to dcMS at the same average power
- The surfaces are significantly smoother when depositing with HiPIMS compared to dcMS

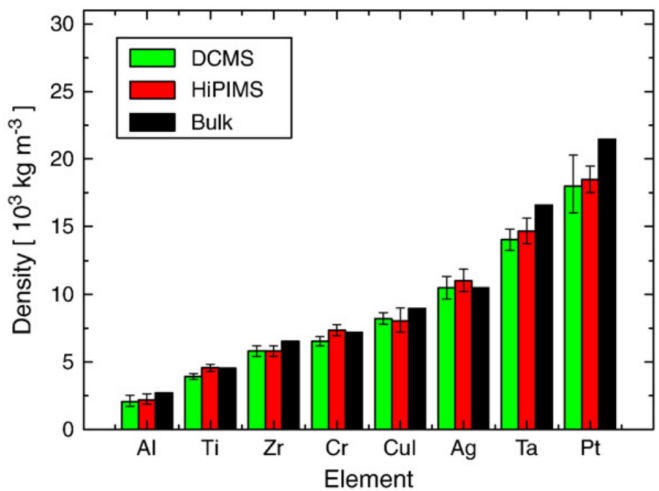

From Samuelsson et al. (2010) SCT **202** 591

Thin film deposition

- TiN as diffusion barriers for interconnects
- HiPIMS deposited films have significantly lower resistivity than dcMS deposited films on SiO_2 at all growth temperatures due to reduced grain boundary scattering
- Thus, ultrathin continuous TiN films with superior electrical characteristics and high resistance towards oxidation can be obtained with HiPIMS at reduced temperatures

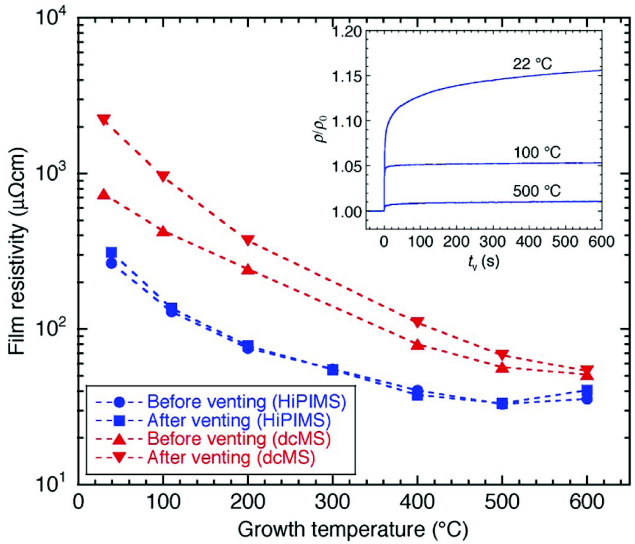

From Magnus et al. (2012) IEEE EDL **33** 1045

Thin film deposition

- There is a drawback
- The deposition rate is lower for HiPIMS when compared to dcMS operated at the same average power
- The HiPIMS deposition rates are typically in the range of 30 – 85% of the dcMS rates depending on target material
- Many of the ions of the target material are attracted back to the target surface by the cathode potential

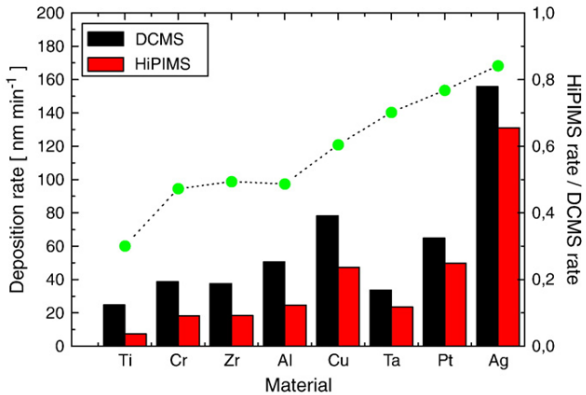

From Samuelsson et al. (2010) SCT **202** 591

The ionization region model (IRM)

Ionization region model

- The ionization region model (IRM) is a time-dependent volume averaged plasma chemical model of the ionization region (IR) of the HiPIMS discharge
- The IRM gives the temporal evolution of the densities of ions, neutrals and electrons
- The IR is defined as an annular cylinder with outer radii r_{c2}, inner radii r_{c1} and length $L = z_2 - z_1$, extends from z_1 to z_2 axially away from the target

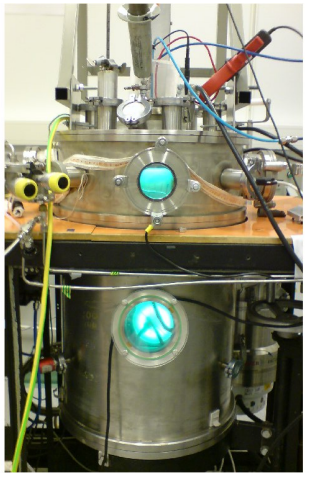

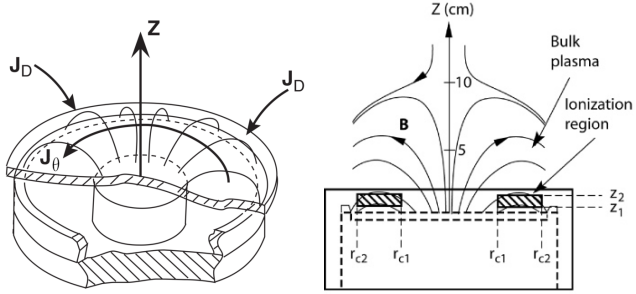

The definition of the volume covered by the IRM

From Raadu et al. (2011) PSST **20** 065007

Detailed model description is given in Huo et al. (2017) JPD **50** 354003

Ionization region model

- The temporal development is defined by a set of ordinary differential equations giving the first time derivatives of
  - the electron energy
  - the particle densities for all the particles (except electrons)
- The species assumed in the non-reactive-IRM are
  - cold electrons e^{C}, hot electrons e^{H}
  - argon atoms $Ar(3s^2 3p^6)$, warm argon atoms in the ground state Ar^{W}, hot argon atoms in the ground state Ar^{H}, Ar^{m} ($1s_5$ and $1s_3$) (11.6 eV), argon ions Ar^{+} (15.76 eV), doubly ionized argon ions Ar^{2+} (27.63 eV)
  - Metal atoms, sometimes metastable states, metal ion M^{+}, and doubly ionized metal ions M^{2+}

Detailed model description is given in Huo et al. (2017), JPD **50** 354003

Ionization region model

- As an example the particle balance equation for the metal ion M^+ is

$$\frac{\mathrm{d}n_{\mathrm{M}^+}}{\mathrm{d}t} = \underbrace{k^{\mathrm{c}}_{\mathrm{iz,M}} n_{\mathrm{e}} n_{\mathrm{M}} + k^{\mathrm{h}}_{\mathrm{iz,M}} n_{\mathrm{e}} n_{\mathrm{M}}}_{\text{electron impact ionization}} + \underbrace{k_{\mathrm{P,iz}} n_{\mathrm{Ar^m}} n_{\mathrm{M}}}_{\text{Penning ionization}}$$

$$+ \underbrace{k_{\mathrm{chexc},1} n_{\mathrm{M}} n_{\mathrm{Ar}^+} + k_{\mathrm{chexc},2} n_{\mathrm{M}^{2+}} n_{\mathrm{Ar}}}_{\text{charge exchange}} - \underbrace{k^{\mathrm{c}}_{\mathrm{iz,M}^+} n_{\mathrm{e}} n_{\mathrm{M}^+} - k^{\mathrm{h}}_{\mathrm{iz,M}^+} n_{\mathrm{e}} n_{\mathrm{M}^+}}_{\text{electron impact ionization to create } \mathrm{M}^{2+}}$$

$$- \underbrace{\frac{\Gamma^{\mathrm{RT}}_{\mathrm{M}^+} + \Gamma^{\mathrm{BP}}_{\mathrm{M}^+}(S_{\mathrm{IR}} - S_{\mathrm{RT}})}{\mathcal{V}_{\mathrm{IR}}}}_{\text{ion flux out of the ionization region}}$$

Ionization region model

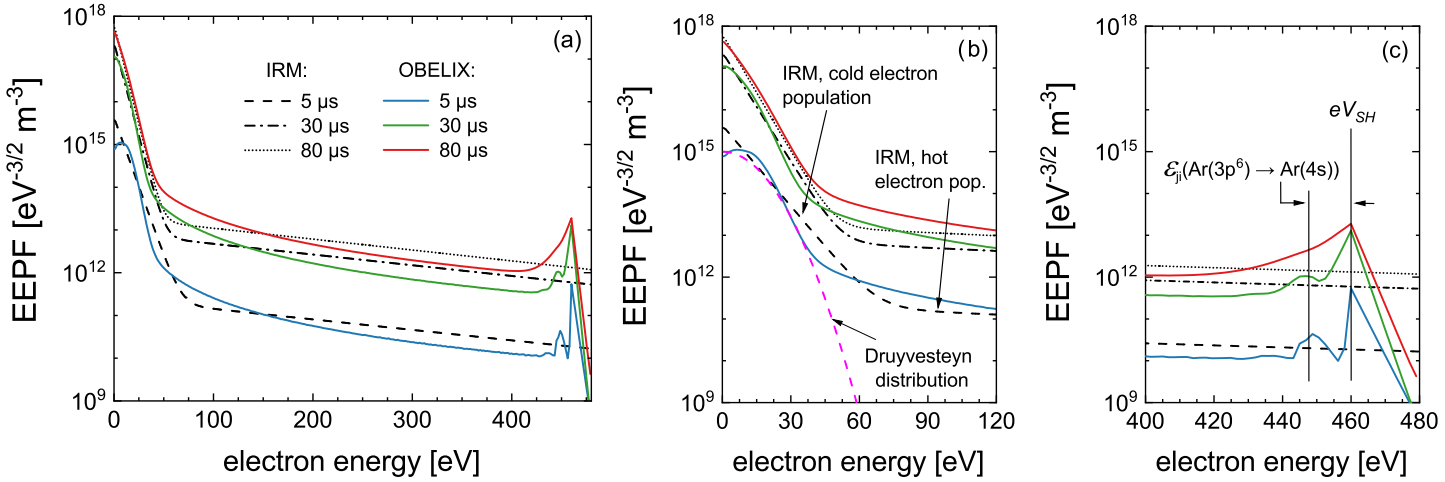

Rudolph et al. (2021) PSST **30** 045011

- The IRM uses two sets of rate coefficients, one for a cold and another for a hot electron group
- The rate coefficients are determined assuming a Maxwellian EEDF and fit in the electron temperature range:
  - 1 – 7 eV cold or primary electrons
  - 200 – 1000 eV hot or secondary electrons

Ionization region model

- The IRM is a semi-empirical discharge model and requires the measured discharge current and voltage waveforms
- The IRM has three unknown fitting parameters
  - the ion back-attraction probability for the metal ions $\beta_{\mathrm{t,pulse}}$ and gas ions $\beta_{\mathrm{g,pulse}}$
  - the potential drop across the IR $f = V_{\mathrm{IR}}/V_{\mathrm{D}}$
  - the electron recapture probability $r = 0.7$
- This leaves the ($\beta_{\mathrm{t,pulse}}$, f) parameter space to be explored through the model fitting procedure – the blue zones in the fitting map indicate the smallest mean square error

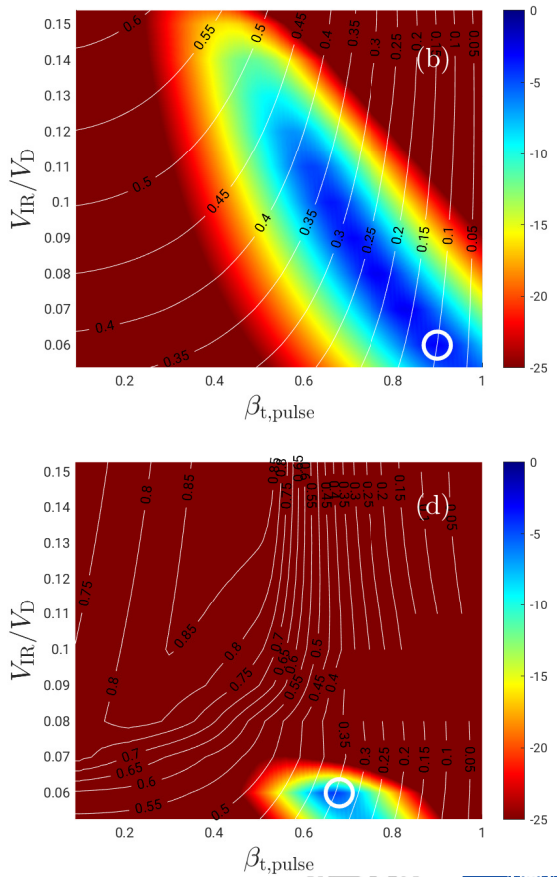

Tungsten target from Suresh Babu et al. (2022) PSST **31** 065009

Ionization region model

- The temporal evolution of the neutral and ion densities in a discharge with tungsten target
- The ground state working gas argon atoms dominate the discharge and its density decreases steadily to a minimum at the end of the pulse – working gas rarefaction
- Initially, the Ar^+ ion is the dominating ion but soon the W^+ ion takes over and remains the dominating ion towards the end of the pulse

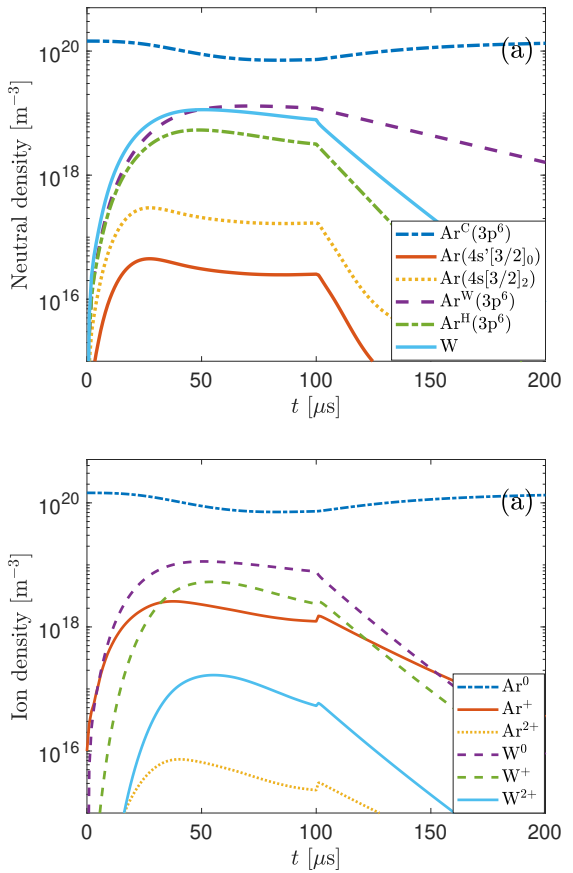

From Suresh Babu et al. (2022) PSST **31** 065009

Ionization region model

- The temporal evolution of the discharge current composition at the target surface
- The initial peak in the discharge current is due to Ar^+ ions
- Later W^+ ions take over as the dominating charged heavy species, as the initial Ar^+ peak decays
- This is more pronounced for the higher discharge voltages as the contribution of the W^+ ions to the total discharge current at the target surface increases with increased discharge voltage

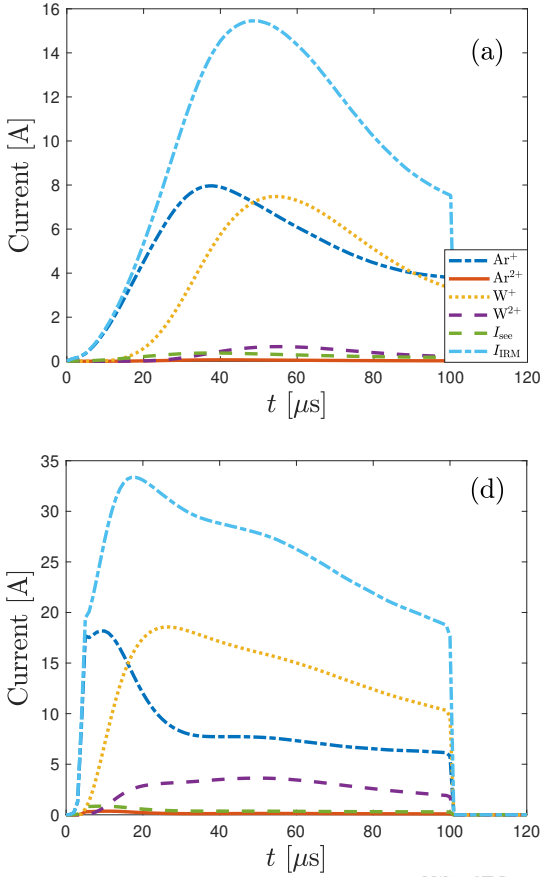

From Suresh Babu et al. (2022) PSST **31** 065009

Ionization region model

- The ionization probability α_t increases with increased discharge voltage
- The back-attraction probability $\beta_{t,pulse}$ decreases with increased discharge voltage
- The peak discharge current increases with increased discharge voltage
- Earlier we have argued that the ionization probability depends only on the peak discharge current and increases with increased peak discharge current

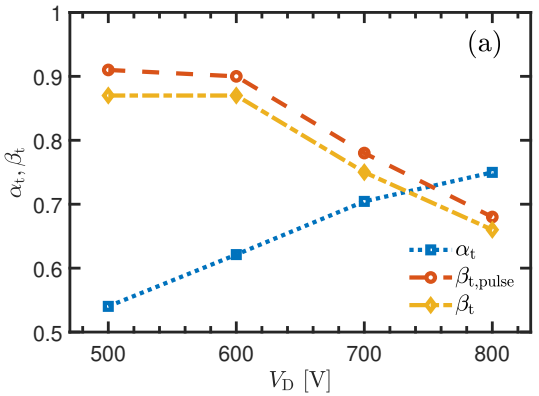

From Suresh Babu et al. (2022) PSST **31** 065009

Rudolph et al. (2022) JPD **55** 015202

Ionization region model

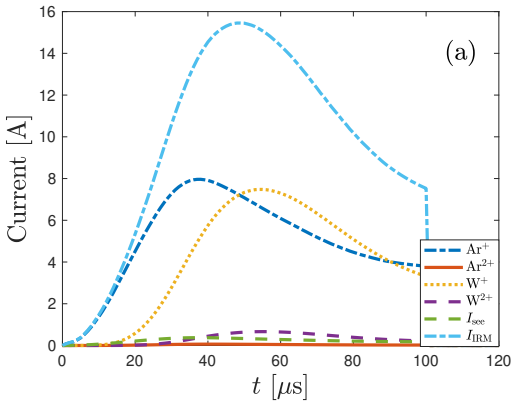

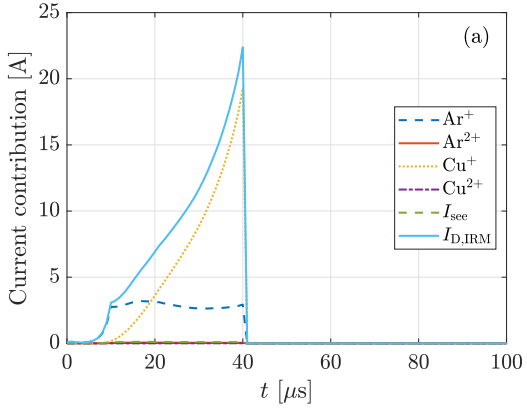

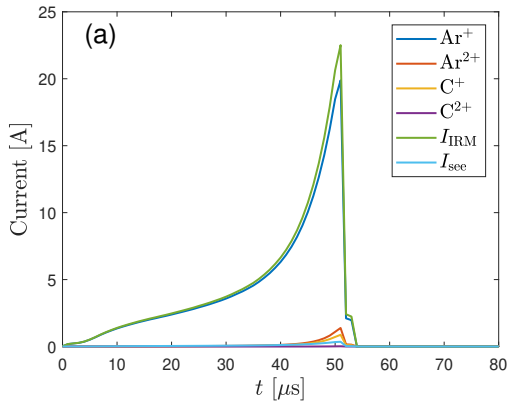

W: PSST (2022) **31** 065009

Cu: SCT (2022) **442** 128189

C: PSST (2021) **30** 115017

- The temporal evolution of the discharge current composition at the target surface for three different targets
- With Cu target Cu^+ ions dominate, with graphite target Ar^+ ions dominate

Working gas rarefaction

Working gas rarefaction

- The sputtered species enter the discharge at considerable energy, which is determined by the cohesive energy of the solid target
- The interaction between the energetic sputtered particles and the working gas atoms can lead to a reduction in the working gas density – as has been observed experimentally in the HiPIMS discharge
- The maximum in the degree of working gas rarefaction, determined by the IRM, for various target materials versus the peak discharge current density $J_{\mathrm{D,peak}}$

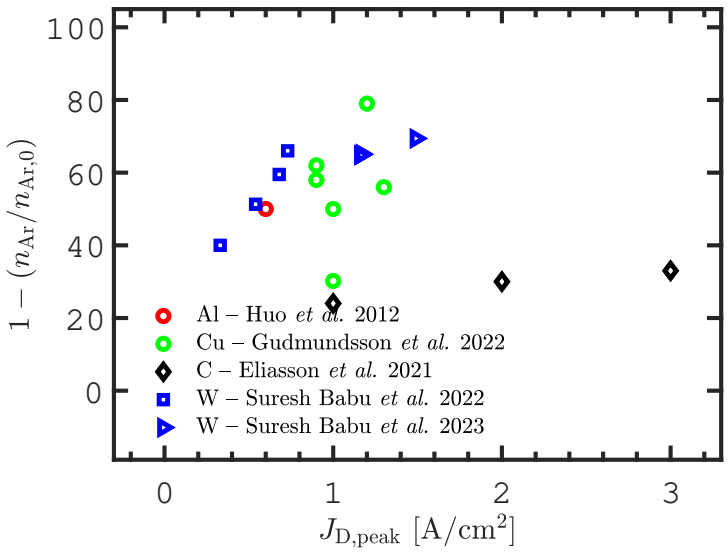

From Barynova et al. to be submitted

Working gas rarefaction

- HiPIMS discharge with graphite target and $J_{\mathrm{D,peak}} = 3$ A cm^{-2}

  Eliasson et al. (2021) PSST **30** 115017

- Argon atoms are lost mainly through electron impact ionization by primary and secondary electrons
- Contributions of kick-out and charge-exchange are negligible
- Diffusion contributes to a net loss of argon atoms during the pulse, but to a flow into the ionization region after the pulse is off

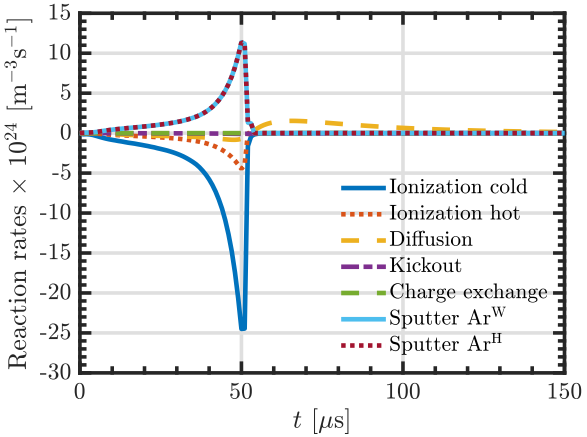

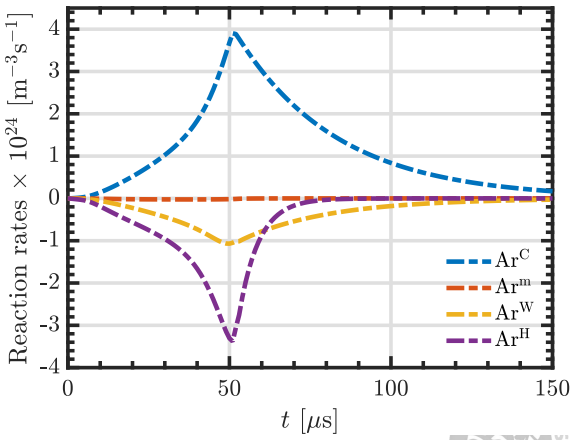

From Barynova et al. to be submitted

Working gas rarefaction

- HiPIMS discharge with tungsten target and $J_{\mathrm{D,peak}} = 0.54$ A cm^{-3}

  Suresh Babu et al. (2022) PSST **31** 065009

- The main contributor to the loss of argon atoms from the IR is kick-out by tungsten atoms sputtered from the target (39 – 48 % contribution)
- The second most important loss process is electron impact ionization by secondary electrons followed by electron impact ionization by the primary electrons

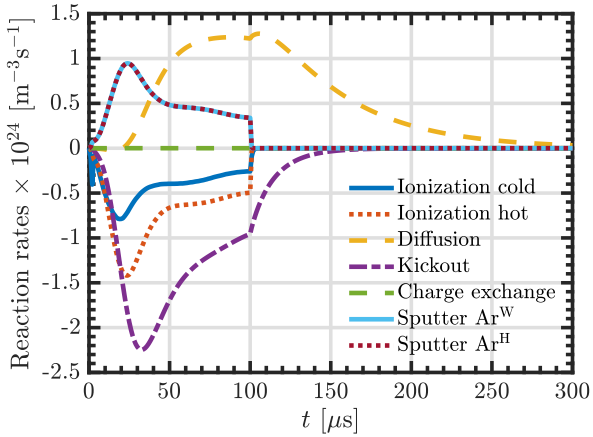

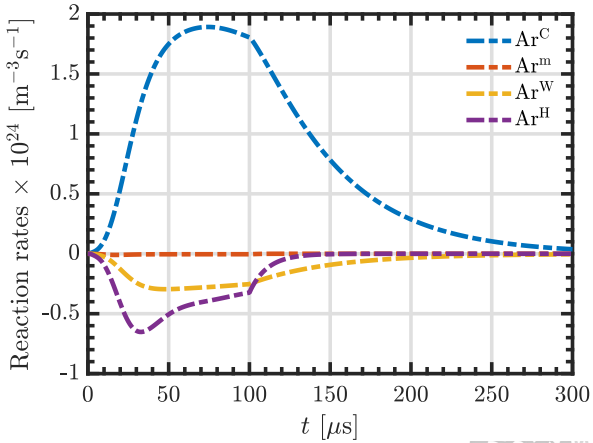

From Barynova et al. to be submitted

Working gas rarefaction

- The relative contributions of the various processes to working gas rarefaction varies greatly depending on the target material
- The various contributions versus the atomic mass of the target material for $J_{\mathrm{D,peak}} \sim 1$ A/cm^2
- Electron impact ionization by primary electrons is rather significant for a graphite target, but its role decreases with increased atomic mass
- The role of kick-out, or the sputter wind, increases with increased mass of the target atom

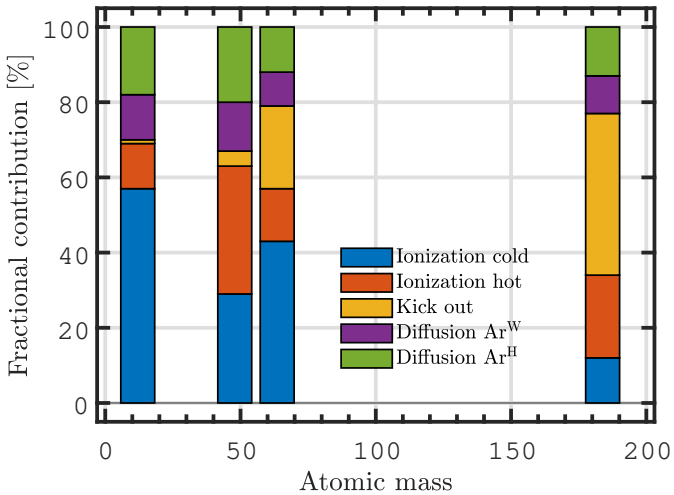

From Barynova et al. to be submitted

Electron power absorption

Electron power absorption

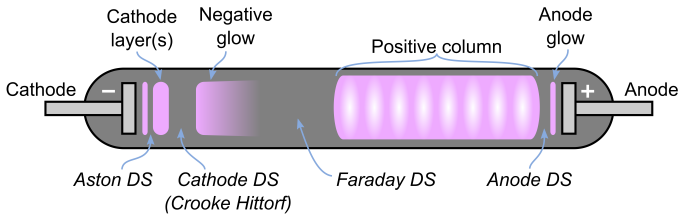

T. J. Petty, LPGP, Université Paris Sud

Gudmundsson and Hecimovic (2017) PSST **26** 123001

- A dc discharge with a cold cathode is sustained by secondary electron emission from the cathode due to ion bombardment
- The discharge current at the target consists of electron current I_e and ion current I_i or

$$I_D = I_e + I_i = I_i(1 + \gamma_{see})$$

where γ_{see} is the secondary electron emission coefficient

- Note that $\gamma_{see} \sim 0.05 - 0.2$ for most metals, so at the target ion current dominates

Electron power absorption

- These secondary electrons are accelerated in the cathode dark space
- They must produce sufficient number of ions to release more electrons from the cathode
- The number of electron-ion pairs created by each secondary electron is then

$$\mathcal{N} \approx \frac{V_{\mathrm{D}}}{\mathcal{E}_{\mathrm{c}}}$$

where $\mathcal{E}_{\mathrm{c}}$ is the energy loss per electron-ion pair created

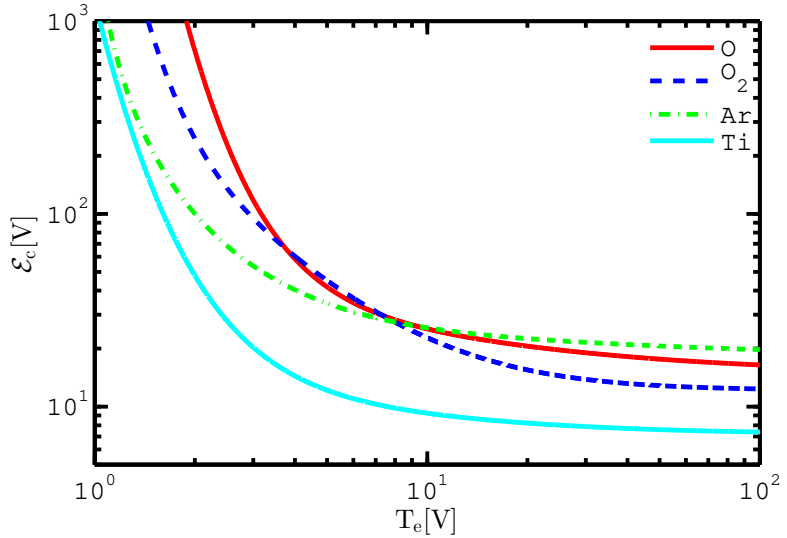

Gudmundsson et al. (2016) PSST **25** 065004

Electron power absorption

- In magnetron sputtering effective secondary electron emission coefficient

$$\gamma_{\mathrm{see,eff}} = m\epsilon_{\mathrm{e}}(1-r)\gamma_{\mathrm{see}}$$

where r is the recapture probability

- To sustain the discharge the condition

$$\gamma_{\mathrm{see,eff}}\mathcal{N} = 1$$

defines the minimum voltage

$$V_{\mathrm{D,min}} = \frac{\mathcal{E}_{\mathrm{c}}}{\beta\gamma_{\mathrm{see,eff}}}$$

referred to as Thornton equation

Magnetron sputtering: basic physics and application to cylindrical magnetrons

John A. Thornton

Telic Corporation, 1631 Colorado Avenue, Santa Monica, California 90404

(Received 22 September 1977; accepted 7 December 1977)

Magnetron sputtering sources can be defined as diode devices in which magnetic fields are used in concert with the cathode surface to form electron traps which are so configured that the **E**×**B** electron-drift currents close on themselves. Coaxial cylindrical magnetron sputtering sources in which post or hollow cathodes are operated in axial magnetic fields have been reported for a number of years. However, their performance is limited by end losses. A remarkable performance is achieved when the end losses are eliminated by proper shaping of the magnetic field or by using suitably placed electron-reflecting surfaces. High currents and sputtering rates can be obtained, nearly independent of voltage, even at low pressures. This characterizes what has been defined as the *magnetron mode* of operation. This paper reviews the basic principles that underly the operation of dc sputtering sources in the magnetron mode with particular emphasis on cylindrical magnetrons. The important attributes of these devices as sputtering sources are also reviewed.

PACS numbers: 81.15.−z, 52.75.−d

Thornton (1978) JVST **15**(2) 171

Electron power absorption

- We can rewrite the Thornton equation

$$\frac{1}{V_{\mathrm{D}}} = \frac{\beta m \epsilon_{\mathrm{e}} (1 - r)}{\mathcal{E}_{\mathrm{c}}} \gamma_{\mathrm{see}}$$

- A plot of the inverse discharge voltage $1/V_{\mathrm{D}}$ against γ_{see} should then give a straight line through the origin
- Depla et al. measured the discharge voltage for 18 different target materials
- It can be seen that a straight line indeed results, but that it does not pass through the origin

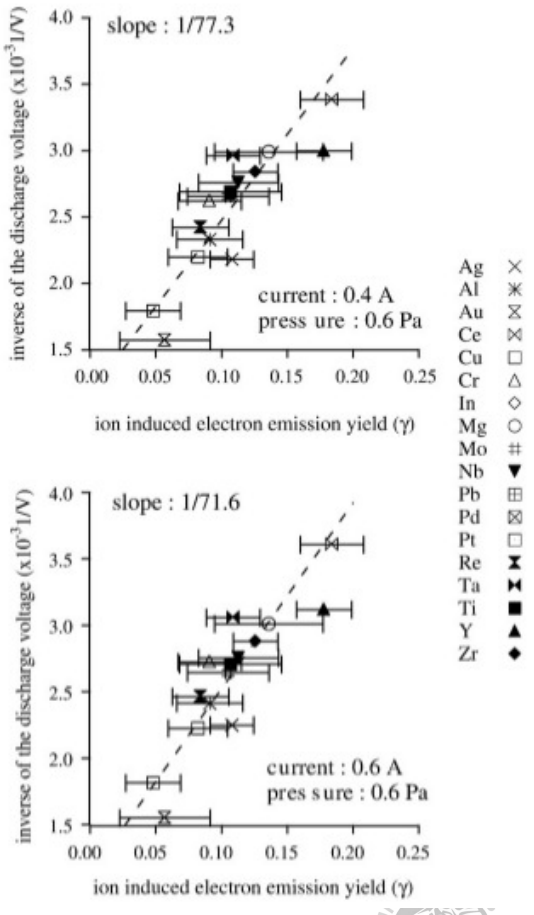

From Depla et al. (2009) TSF **517** 2825

Electron power absorption

- We have proposed that the intercept is due to Ohmic heating
- We can now write the inverse discharge voltage $1/V_{\mathrm{D}}$ in the form of a generalized Thornton equation

$$\frac{1}{V_{\mathrm{D}}} = \underbrace{\frac{\beta \epsilon_{\mathrm{e}}^{\mathrm{H}} m (1-r)(1-\delta_{\mathrm{IR}})}{\mathcal{E}_c^{\mathrm{H}}}}_{a} \gamma_{\mathrm{see}} + \underbrace{\frac{\epsilon_{\mathrm{e}}^{\mathrm{C}} \langle I_{\mathrm{e}}/I_{\mathrm{D}} \rangle_{\mathrm{IR}} \delta_{\mathrm{IR}}}{\mathcal{E}_c^{\mathrm{C}}}}_{b}$$

or

$$\frac{1}{V_{\mathrm{D}}} = a\gamma_{\mathrm{see}} + b$$

- We associate a with hot electrons e^{H}, sheath acceleration
- We associate b with the Ohmic heating process and cold electrons e^{C}

Electron power absorption

- The fraction of the total ionization that is due to Ohmic heating can be obtained directly from the line fit parameters *a* and *b* or as a function of only the secondary electron yield γ_{SE}

$$\frac{\iota_{\text{Ohmic}}}{\iota_{\text{total}}} = \frac{b}{a\gamma_{SE} + b}$$

- The fraction of the discharge voltage that falls over the ionization region

$$\delta_{IR} = \frac{V_{IR}}{V_D} = 0.15 - 0.19$$

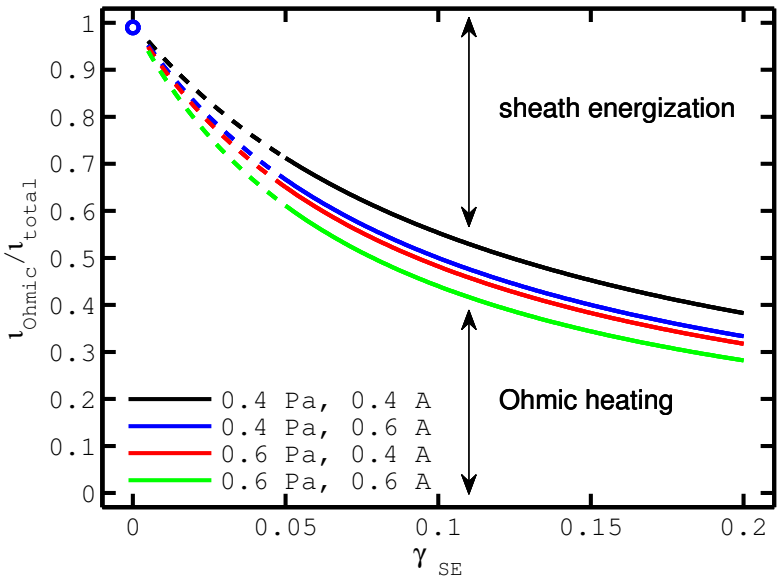

From Brenning et al. (2016) PSST **25** 065024

Electron power absorption

- The presence of a transverse magnetic field enables a potential drop to exist outside the cathode sheath
- A potential V_{SH} falls over the sheath, and the rest of the applied voltage, $V_{\mathrm{IR}} = V_{\mathrm{D}} - V_{\mathrm{SH}}$, falls across the extended pre-sheath, the ionization region (IR), $\delta_{\mathrm{IR}} = V_{\mathrm{IR}}/V_{\mathrm{D}}$
- Ohmic heating, the dissipation of locally deposited electric energy $\mathbf{J}_{\mathrm{e}} \cdot \mathbf{E}$ to the electrons in the plasma volume outside the sheath

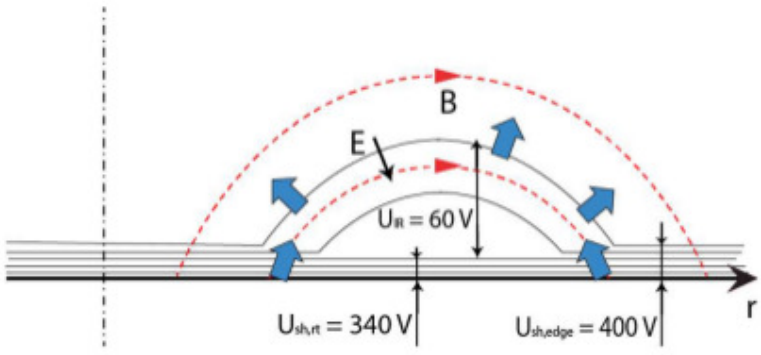

From Brenning et al. (2016) PSST **25** 065024

Electron power absorption

- Applying the ionization region model (IRM) to a HiPIMS discharge
- For the Al target, Ohmic heating is in the range of 87 % (360 V) to 99 % (1000 V)
- The domination of Al^{+}-ions, which have zero secondary electron emission yield, has the consequence that there is negligible sheath energization
- The ionization threshold for twice ionized Al^{2+}, 18.8 eV, is so high that few such ions are produced

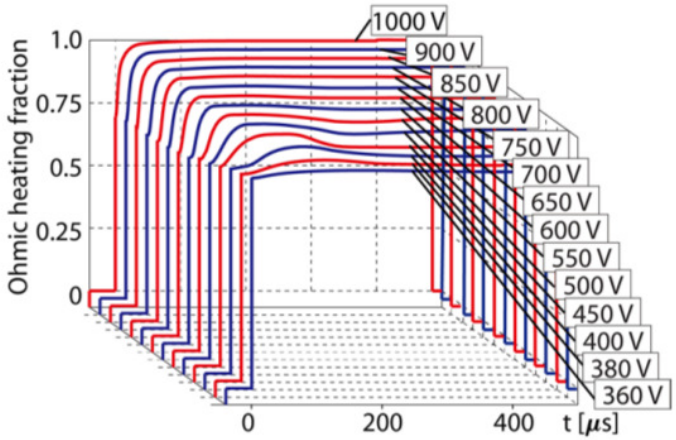

From Huo et al. (2017) JPD **50** 354003

Electron power absorption

- For a Ti target Ohmic heating is about 92 %
  - Both Ar^{+} and Ti^{2+}-ions contribute to creation of secondary electrons
- For Ti target in Ar/O_2 mixture
  - In the metal mode Ohmic heating is found to be 90 % during the plateau phase of the discharge pulse
  - For the poisoned mode Ohmic heating is 70 % with a decreasing trend, at the end of the pulse

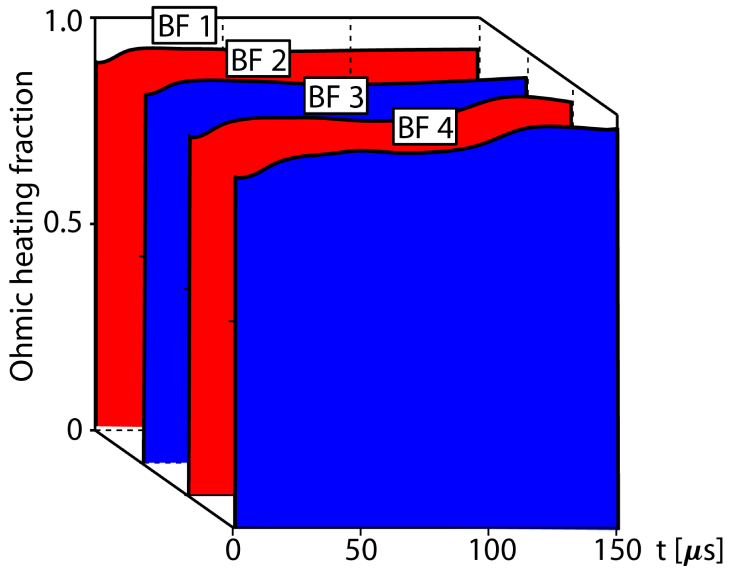

From Huo et al. (2017) JPD **50** 354003

Electron power absorption

- There are indications that the ratio of Ohmic heating to sheath heating changes depending on the magnetic field configuration
- Magnetron assembly with definitions of the parameters B_{rt} and z_{null}, and the distance coordinates z_{C} and z_{E} for the central (C) and the annular edge (E) magnet with respect to their closest position to the rear of the target

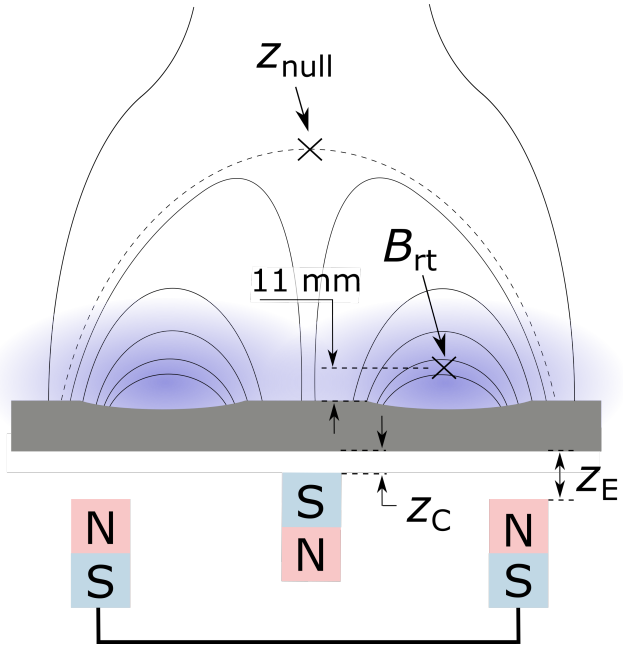

From Rudolph et al. (2022) JPD **55** 015202

Electron power absorption

- To describe the magnetic field we use a constructed parameter $z_{\mathrm{gap}} = z_{\mathrm{C}} + z_{\mathrm{E}}$ instead of the 'classical' magnetic field parameters B_{rt} and z_{null}
- We analyze discharges with Ti target with adjustable confining magnetic field

Hajihoseini et al. (2019) Plasma **2** 201

- The total power that is necessary to heat electrons by Ohmic heating is only 10 – 20 % compared to the power needed to heating electrons by the same amount in the sheath

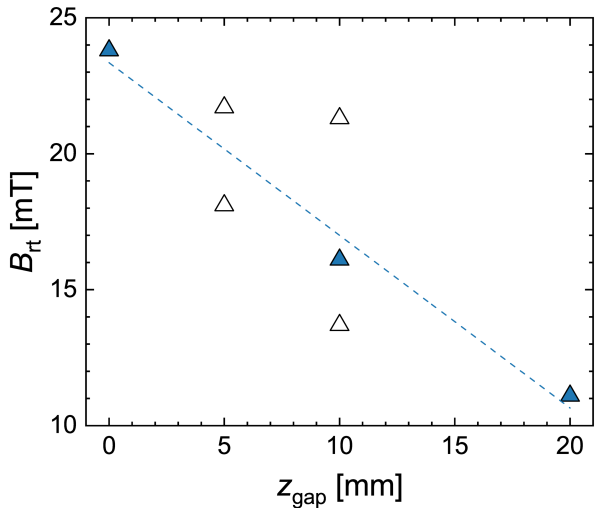

From Rudolph et al. (2022) JPD **55** 015202

Electron power absorption

- $P_{\mathrm{Ohm}}/(P_{\mathrm{Ohm}} + P_{\mathrm{SH}})$ versus the magnetic field parameter z_{gap}
- For increasing z_{gap} (lower magentic field), the fraction $P_{\mathrm{Ohm}}/(P_{\mathrm{Ohm}} + P_{\mathrm{SH}})$ decreases – in line with the increase in pulse power
- $P_{\mathrm{Ohm}}/(P_{\mathrm{Ohm}} + P_{\mathrm{SH}})$ can be regarded as a measure for energy efficiency of a discharge

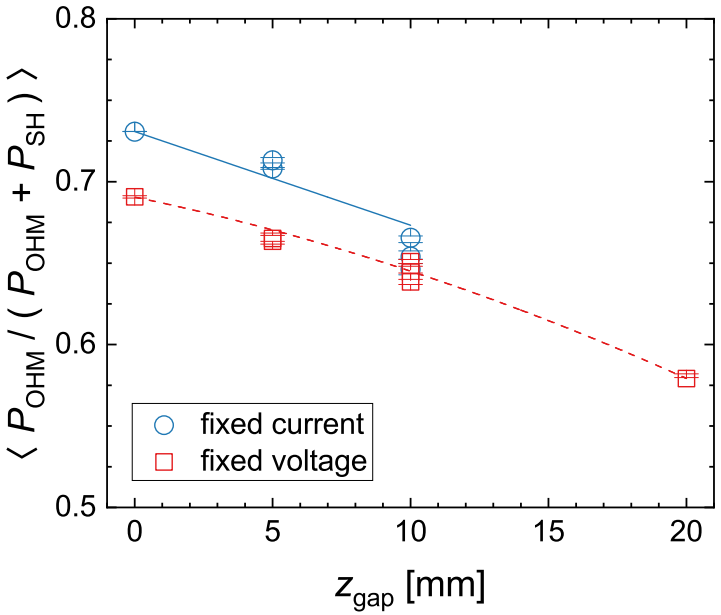

From Rudolph et al. (2022) JPD **55** 015202

Electron power absorption

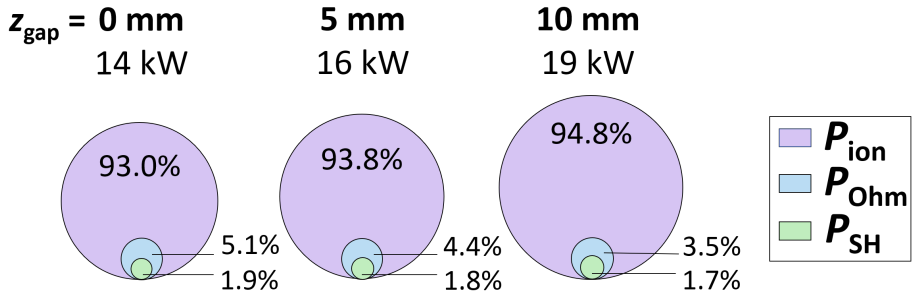

From Rudolph et al. (2022) JPD **55** 015202

- The use of the pulse power for different values of z_{gap}
  - ion acceleration (P_{ion})
  - Ohmic heating (P_{Ohm})
  - sheath energization (P_{SH}).
- Most of the pulse power $\langle P_{pulse} \rangle$ is used to accelerate ions and this power is finally dissipated in the target as heat
- The fraction of the pulse power that is absorbed by the electrons decreases for higher values of z_{gap} and more energy is spent on heating up the target

Deposition rate vs ionized flux fraction

Deposition rate

- The Ti deposition rate and the ionized flux fraction are measured using a gridless ion meter (m-QCM)

  Kubart et al. (2014) *SCT* **238** 152

- The ion meter is mounted on a probe holder which can be moved around within the chamber
- The Ar working gas pressure was set to 1 Pa
- In all cases the pulse width was 100 μs at an average power of 300 W
- The confining magnetic field is varied by moving the magnets

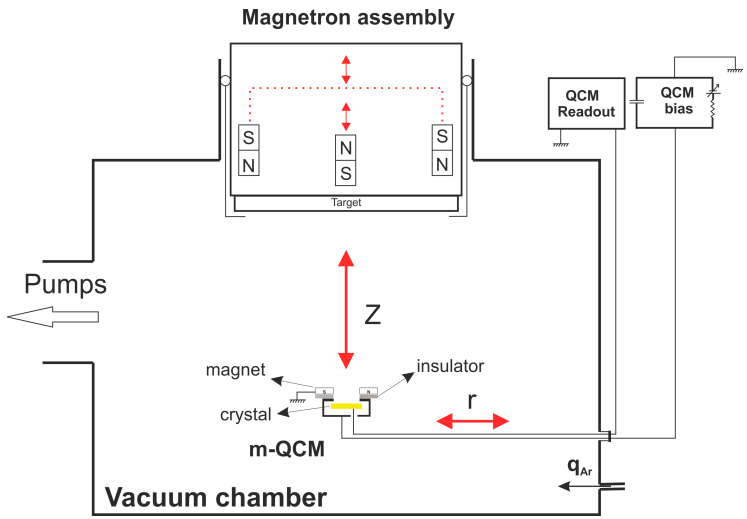

From Hajihoseini et al. (2019) *Plasma* **2** 201

Deposition rate

- The Ti deposition rate recorded at substrate position using a gridless ion meter (m-QCM)
  - **dcMS**
    +10% with decreasing |**B**|
    (but no obvious trend)
  - **HiPIMS fixed voltage**
    +110% with decreasing |**B**|
  - **HiPIMS fixed peak current**
    +40% with decreasing |**B**|
- In HiPIMS operation the deposition rate increases with decreasing |**B**|

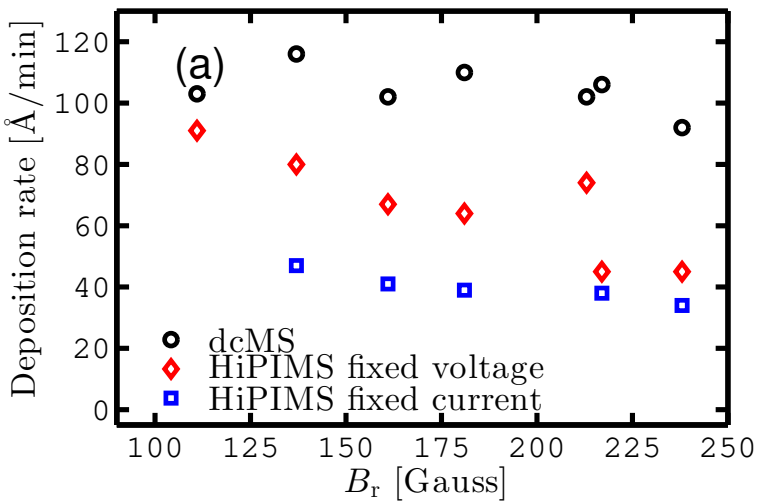

From Gudmundsson (2020) *PSST* **29**(11) 113001

based on Hajihoseini et al. (2019) *Plasma* **2** 201

Deposition rate – Ionized flux fraction

- Ionized flux fraction recorded
  - **dcMS**
    Always around 0 %
    (Kubart et al., 2014)
  - **HiPIMS fixed voltage**
    -75% with decreasing $|\mathbf{B}|$
  - **HiPIMS fixed peak current**
    $+50\%$ with decreasing $|\mathbf{B}|$
- The ionized flux fraction decreases with decreasing $|\mathbf{B}|$ when the HiPIMS discharge is operated in fixed voltage mode but increases in fixed peak current mode
- Opposing trends

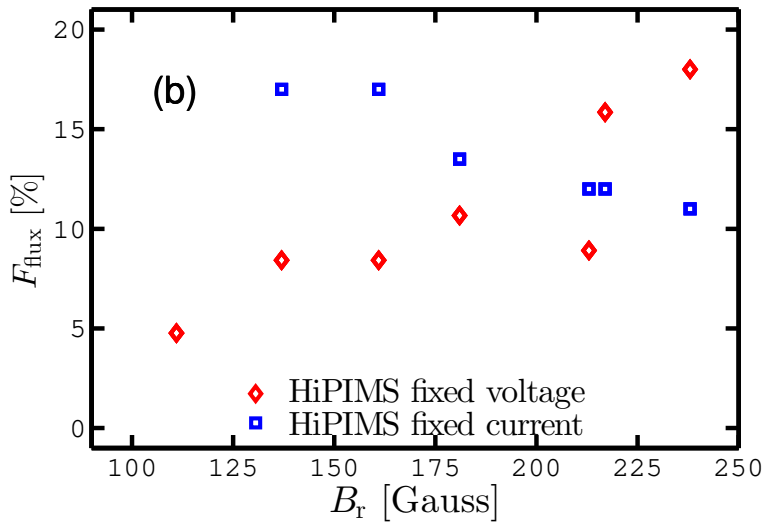

From Gudmundsson (2020) *PSST* **29**(11) 113001

based on Hajihoseini et al. (2019) *Plasma* **2** 201

Deposition rate – α_t and β_t

- Low deposition rate is the main drawback of this sputter technology and hampers its use for industrial applications
- The main reason for the low deposition rate of the HiPIMS discharge is suggested to be due to the back-attraction of the ions of the sputtered species to the cathode target
- Increased deposition rate in HiPIMS often comes at the cost of a lower ionized flux fraction of the sputtered material
- Two internal parameters are of importance
  - α_t – ionization probability
  - β_t – back-attraction probability

Deposition rate – α_t and β_t

- We can relate the measured quantities normalized deposition rate $F_{\mathrm{DR,sput}}$ and the ionized flux fraction $F_{\mathrm{ti,flux}}$

$$F_{\mathrm{DR,sput}} = \frac{\Gamma_{\mathrm{DR}}}{\Gamma_0} = (1 - \alpha_t \beta_t)$$

$$F_{\mathrm{ti,flux}} = \frac{\Gamma_{\mathrm{DR,ions}}}{\Gamma_{\mathrm{DR,sput}}} = \frac{\Gamma_0 \alpha_t (1 - \beta_t)}{\Gamma_0 (1 - \alpha_t \beta_t)} = \frac{\alpha_t (1 - \beta_t)}{(1 - \alpha_t \beta_t)}$$

to the internal parameters back attraction probability β_t

$$\beta_t = \frac{1 - F_{\mathrm{DR,sput}}}{1 - F_{\mathrm{DR,sput}}(1 - F_{\mathrm{ti,flux}})}$$

and ionization probability α_t

$$\alpha_t = 1 - F_{\mathrm{DR,sput}}(1 - F_{\mathrm{ti,flux}})$$

Hajihoseini et al. (2019) *Plasma* **2** 201 and later refined by Rudolph et al. (2021) JAP **129** 033303

Deposition rate – Optimization

- There are two measures of how good a HiPIMS discharge is:
  - the fraction $F_{\mathrm{DR,sput}}$ of all the sputtered material that reaches the diffusion region (DR)
  - the fraction $F_{\mathrm{ti,flux}}$ of ionized species in that flux
- There is a trade off between the goals of higher $F_{\mathrm{DR,sput}}$ and higher $F_{\mathrm{ti,flux}}$
- The figure shows $F_{\mathrm{DR,sput}}$ and $F_{\mathrm{ti,flux}}$ as functions of α_{t} at assumed fixed value of $\beta_{\mathrm{t}} = 0.87$

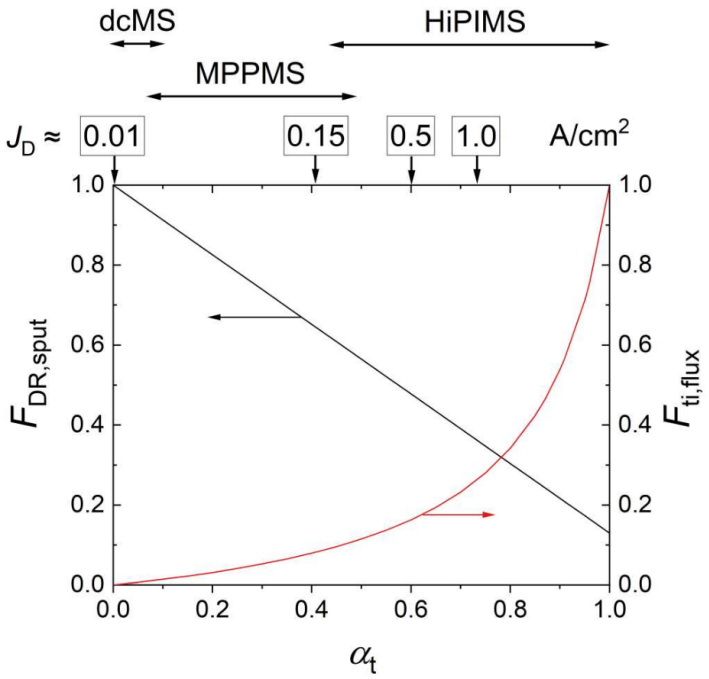

From Brenning et al. (2020) *JVSTA* **38** 033008

Deposition rate – Optimization

- For a particular application an ionized flux fraction of 30 % is suitable but $0.8 \leq \beta_t \leq 0.95$
- If the back-attraction can be reduced to $\beta_t = 0.8$ the deposition rate is increased
- The solid lines show that reducing the back-attraction to $\beta_t = 0.8$ where $\alpha_t = 0.69$ is sufficient to maintain $F_{\mathrm{ti,flux}} = 0.30$ (red circle) $F_{\mathrm{DR,sput}} = 0.45$ or a factor of three increase in the deposition rate
- The question that remains:
  - How can we vary the ionization probability α_t and maybe more importantly the back-attraction probability β_t ?

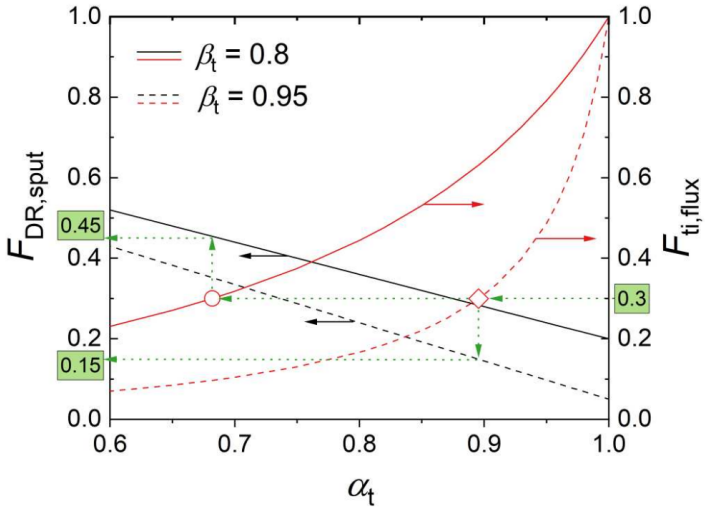

From Brenning et al. (2020) JVSTA **38** 033008

Depostion rate – α_t and β_t

- The internal discharge parameters α_t and β_t from the ionization region model (IRM)
- The ionization probability α_t increases with increased discharge current
- The ion escape fraction $(1 - \beta_t)$ versus the magnetic field strength

From Rudolph et al. (2022) JPD **55** 015202

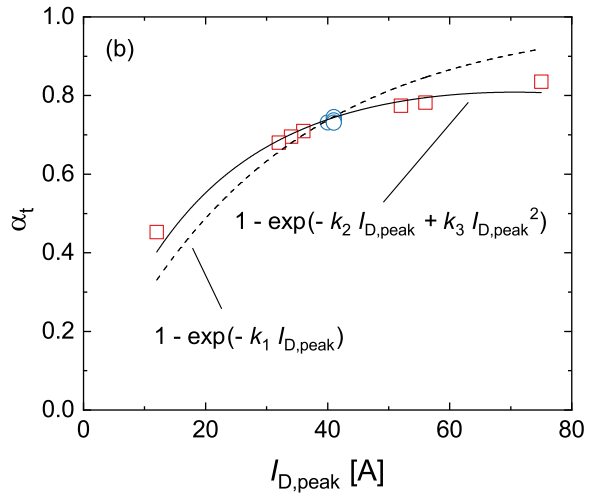

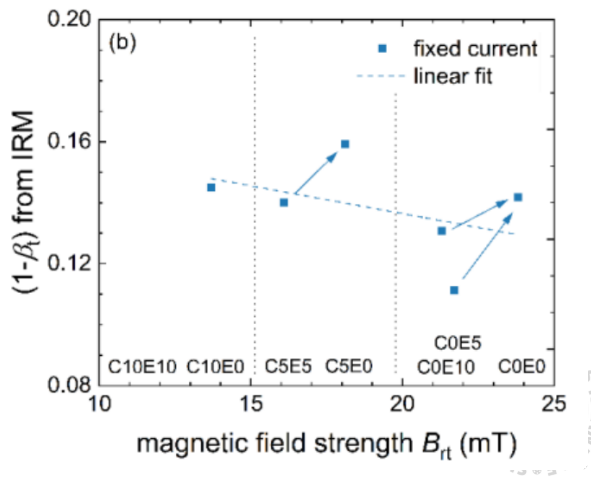

Deposition rate – Pulse length

- For the same average power, shorter pulses give higher deposition rate than longer pulses
- To maintain the same average power the repetition frequency is varied
- Shortening the pulses does not affect the ionized flux fraction, which remains essentially constant
  - with shorter pulses, the afterglow contributes increasingly more to the total deposition rate
  - the ionized flux fraction from the afterglow is typically higher compared to that during the pulse due to absent back-attracting electric field

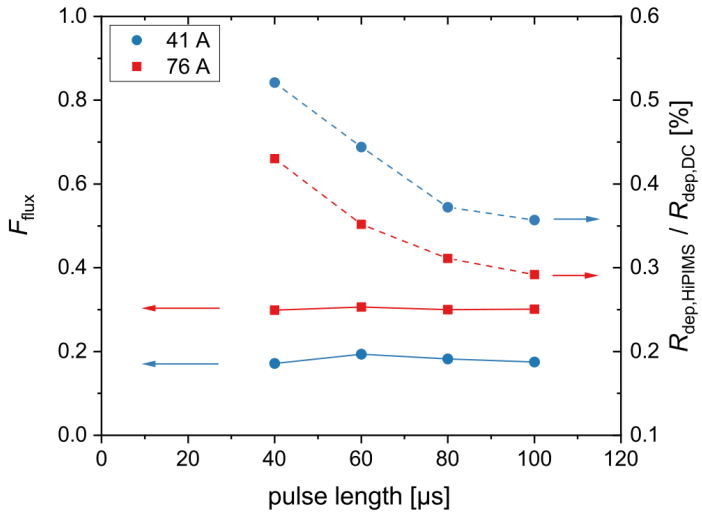

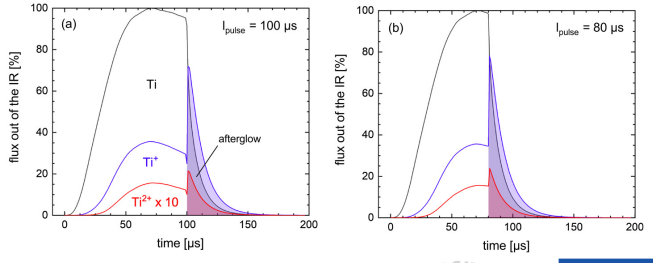

Rudolph et al. (2020) PSST **29** 05LT01

Deposition rate – Pulse length

- By switching-off the cathode potential during the afterglow decreases the effective β_t
- β_t decreases with decreasing pulse length
- The relative contribution of the afterglow ions to the flux toward the DR increases steadily for shorter pulses
- The ionization probability α_t also decreases with a shorter pulse length
- The useful fraction of the sputtered species therefore increases

$$F_{DR,sput} = \frac{\Gamma_{DR}}{\Gamma_0} = (1 - \alpha_t \beta_t)$$

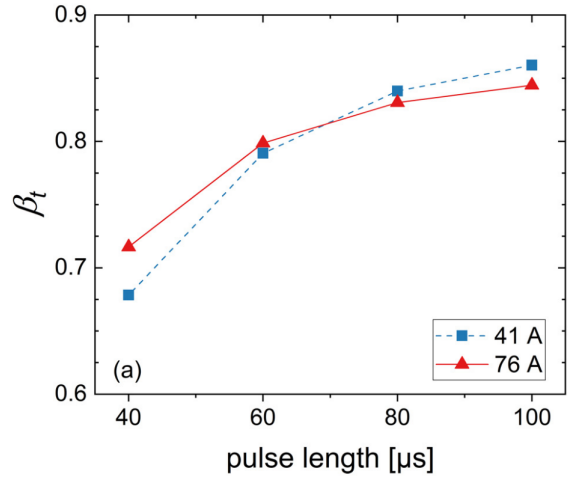

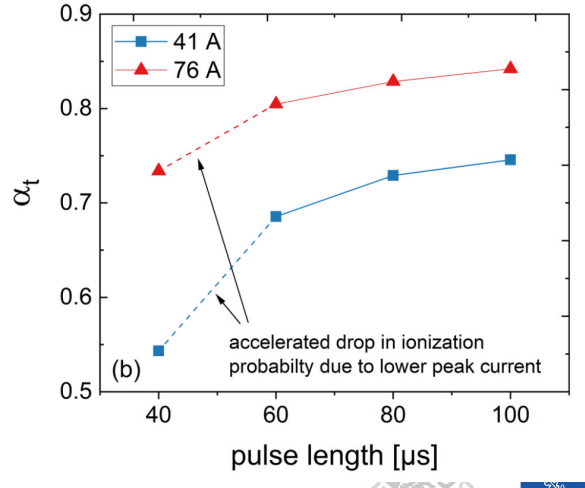

Deposition rate – Pulse length

- These findings have been confirmed experimentally
- 6“ circular target with Ti target
- The pulse length is in the range of 15 – 200 μs, and the peak discharge current density $J_{\mathrm{D,peak}} = 0.37, 0.70, 1.10$ A/cm^2 ajusted the the discharge voltage
- The average sputtering power delivered to the target was kept at 1 kW by adjusting the pulse repetition frequency in the range 85 – 980 Hz

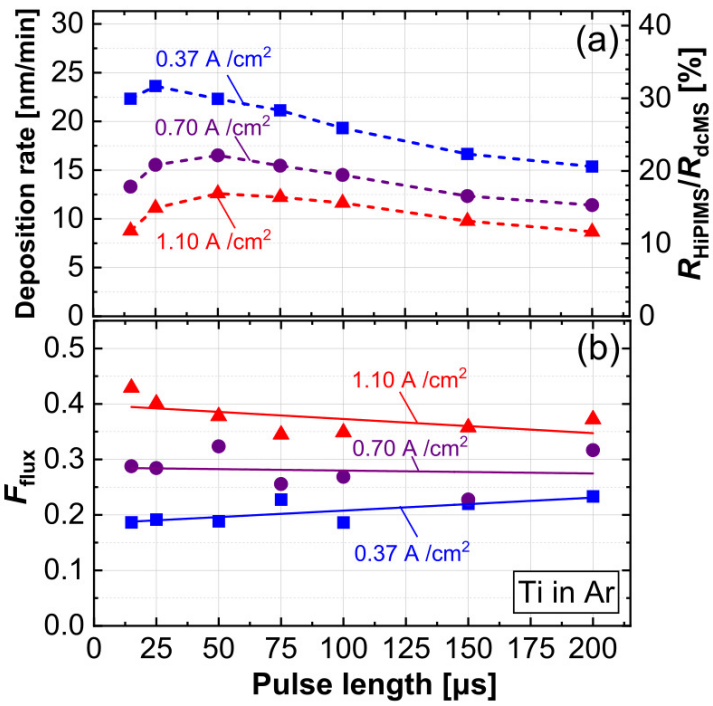

Shimizu et al. (2021) PSST **29** 045006

Recycling in HiPIMS discharges

Recycling in HiPIMS discharges

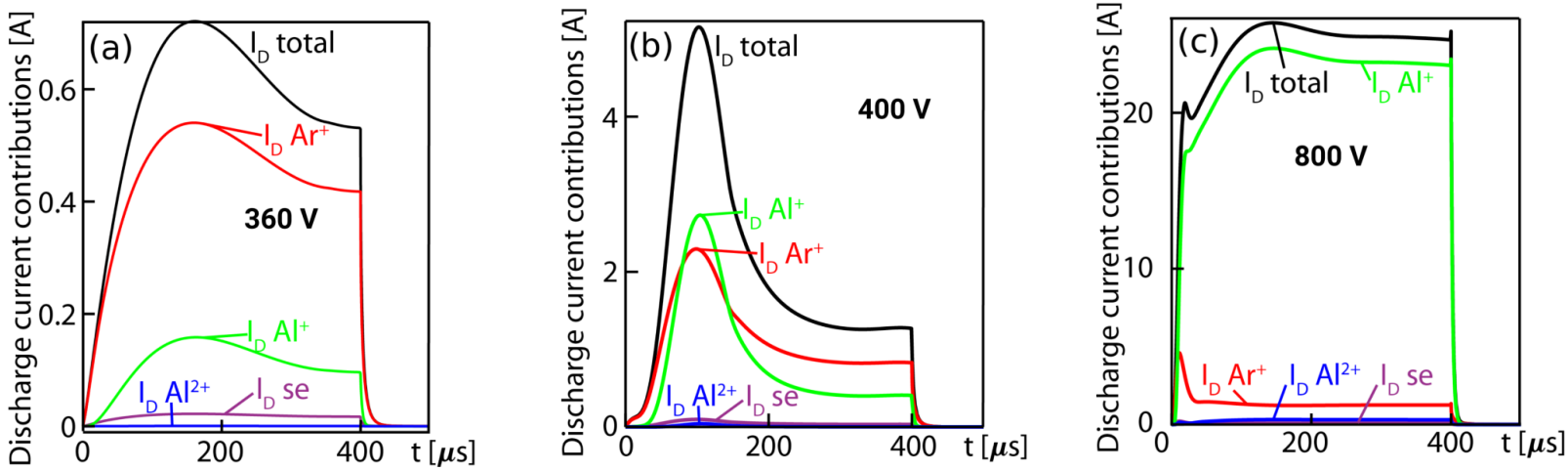

- A **non-reactive** discharge with 50 mm diameter Al target
- Current composition at the target surface

From Huo et al. (2017) JPD **50** 354003

Experimental data from Anders et al. (2007) JAP **102** 113303

Recycling in HiPIMS discharges

- A primary current I_{prim} is defined as ions of the working gas, here Ar^+, that are ionized for the first time and then drawn to the target
- This is the dominating current in dc magnetron sputtering discharges
- This current has a critical upper limit

$$I_{\mathrm{crit}} = S_{\mathrm{RT}} e p_{\mathrm{g}} \sqrt{\frac{1}{2\pi m_{\mathrm{g}} k_{\mathrm{B}} T_{\mathrm{g}}}} = S_{\mathrm{RT}} e n_{\mathrm{g}} \sqrt{\frac{k_{\mathrm{B}} T_{\mathrm{g}}}{2\pi m_{\mathrm{g}}}}$$

- Discharge currents I_{D} above I_{crit} are only possible if there is some kind of recycling of atoms that leave the target, become subsequently ionized and then are drawn back to the target

Anders et al. (2012) JPD **45** 012003

Huo et al. (2014) PSST **23** 025017

Recycling in HiPIMS discharges

- For the 50 mm diameter Al target the critical current is $I_{\mathrm{crit}} \approx 7$ A
- The experiment is operated from far below I_{crit} to high above it, up to 36 A.
- With increasing discharge current I_{prim} gradually becomes a very small fraction of the total discharge current I_{D}
- The current becomes mainly carried by singly charged Al^{+}-ions, meaning that **self-sputter recycling** or the current $I_{\mathrm{SS-recycle}}$ dominates

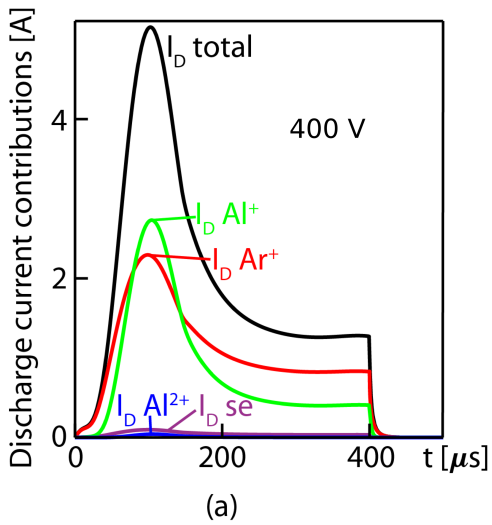

(a)

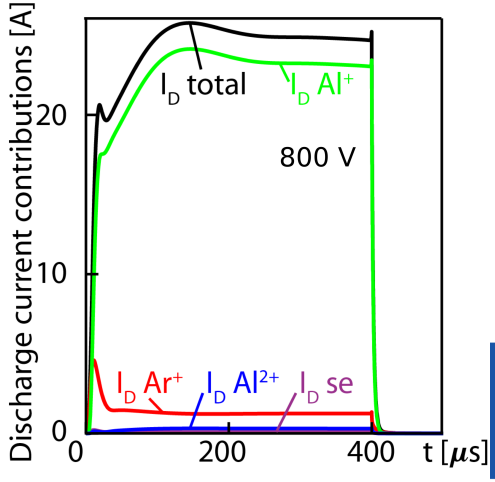

(b)

From Huo et al. (2017) JPD **50** 354003

Experimental data from Anders et al. (2007) JAP **102** 113303

Recycling in HiPIMS discharges

- For discharges with Ti target the peak current is far above the critical current (up to 650 A, while $I_{\mathrm{crit}} \approx 19$ A)
- However, this discharge shows close to a 50/50 combination of **self-sputter recycling** $I_{\mathrm{SS-recycle}}$ and **working gas-recycling** $I_{\mathrm{gas-recycle}}$
- Almost 2/3 of the current to the target is here carried by Ar^{+} and Ti^{2+}-ions, which both can emit secondary electrons upon target bombardment, and this gives a significant sheath energization

From Huo et al. (2017) JPD **50** 354003

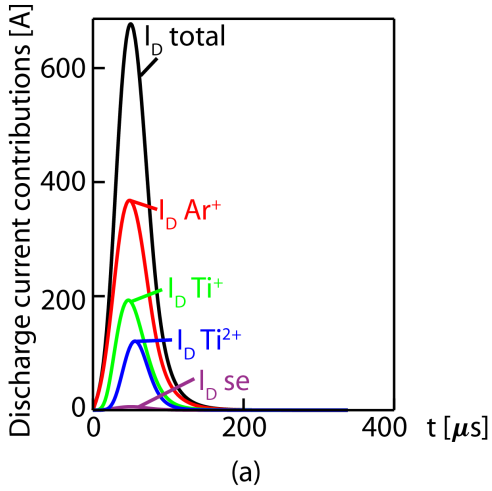

(a)

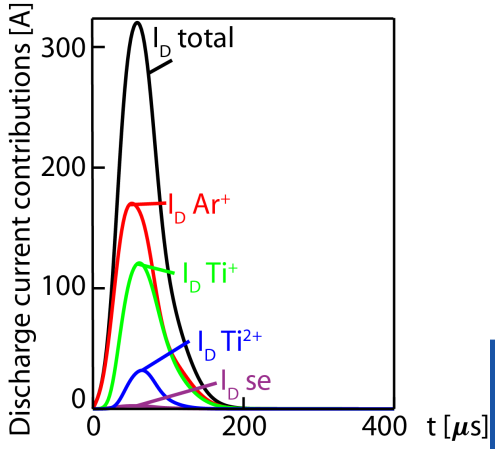

(b)

Recycling in HiPIMS discharges

- The total discharge current is

$$I_D = I_{prim} + I_{gas-recycle} + I_{SS}$$

$$= I_{prim}\left(1 + \frac{\pi_g}{1-\pi_g}\right)\left(1 + \frac{Y_g}{Y_{SS}}\frac{\pi_{SS}}{1-\pi_{SS}}\right)$$

where the working gas-sputtering parameter is

$$\pi_g = \alpha_g \beta_g \xi_{pulse}$$

and the self-sputter parameter

$$\pi_{SS} = \alpha_t \beta_t Y_{SS}$$

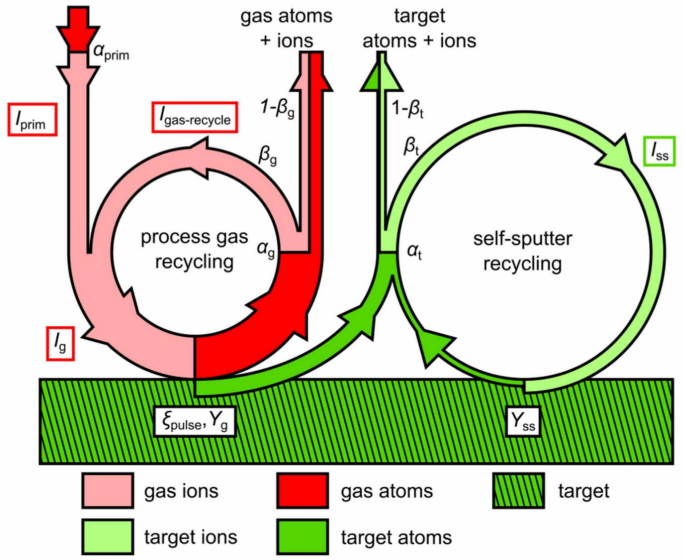

From Brenning et al. (2017) PSST **26** 125003

Recycling in HiPIMS discharges

- With increased discharge voltage the discharge with Al target moves from the dcMS regime to the HiPIMS discharge regime – **type A**
- A discharge with carbon target jumps from the dcMS regime to the HiPIMS regime – both SS recycling and working gas recycling play a role – intermediate **type AB**
- For reactive sputtering of Ti target in poisoned mode working gas recycling dominates – **type B**

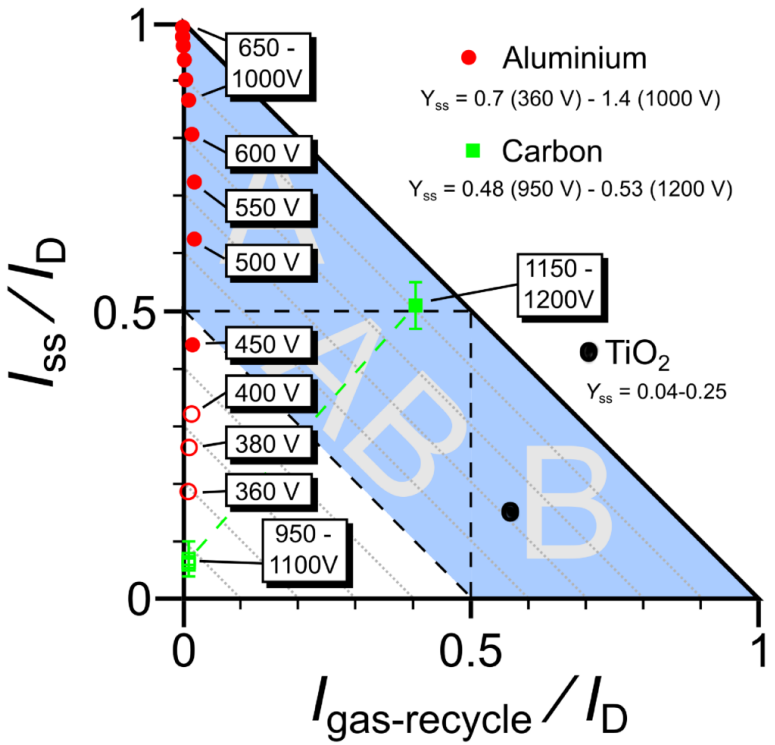

From Brenning et al. (2017) PSST **26** 125003

Recycling in HiPIMS discharges

- Recycling map for five different targets with varying self-sputter yield
  - Cu – $Y_{SS} = 2.6$
  - Al – $Y_{SS} = 1.1$
  - Ti – $Y_{SS} = 0.7$
  - C – $Y_{SS} = 0.5$
  - TiO_2 – $Y_{SS} = 0.04 - 0.25$
- For very high self-sputter yields $Y_{SS} > 1$, the discharges above I_{crit} are of **type A** with dominating **SS-recycling**
- For very low self-sputter yields $Y_{SS} < 0.2$, the discharges above I_{crit} are of **type B** with dominating **working gas recycling**

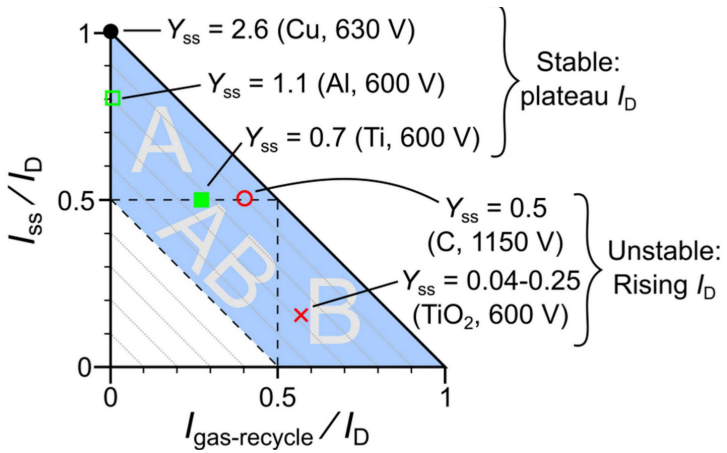

From Brenning et al. (2017) PSST **26** 125003

Recycling in HiPIMS discharges – copper

- The temporal evolution of the discharge current composition at the target surface for a peak discharge current density 2 A/cm^2
- A discharge with 2 inch copper target – $I_{\mathrm{crit}} \approx 3.8$ A
- The Cu^+ ion is the dominating positively charged species in the discharge
- The ionized flux fraction of copper is roughly 32 %

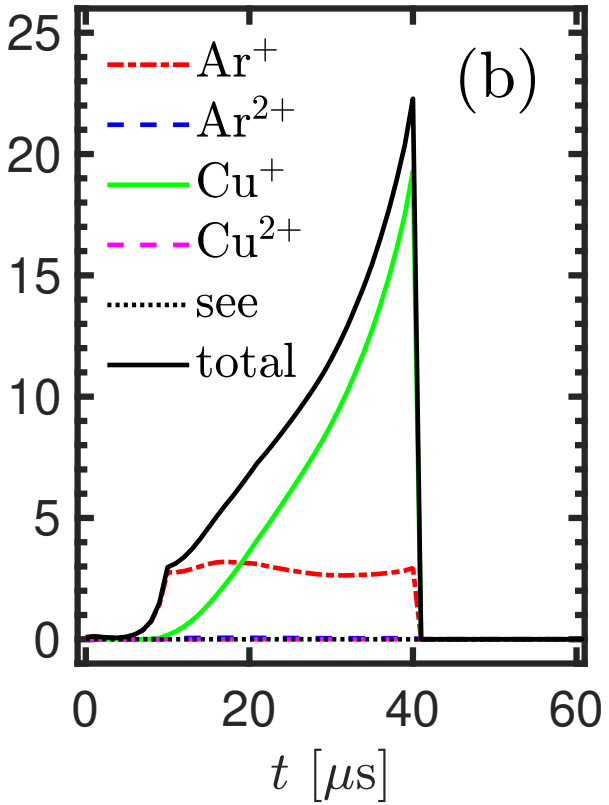

Based on Gudmundsson et al. (2022) 442 126189

Recycling in HiPIMS discharges – carbon

- The temporal evolution of the discharge current composition at the target surface for a peak discharge current density 2 A/cm^2
- A discharge with 2 inch graphite target – $I_{\mathrm{crit}} \approx 7.6$ A
- The Ar^+ ion is the dominating positively charged species in the discharge
- Less than 5 % of the total discharge current is carried by C^+ ions
- The ionized flux fraction of carbon is roughly 2 %

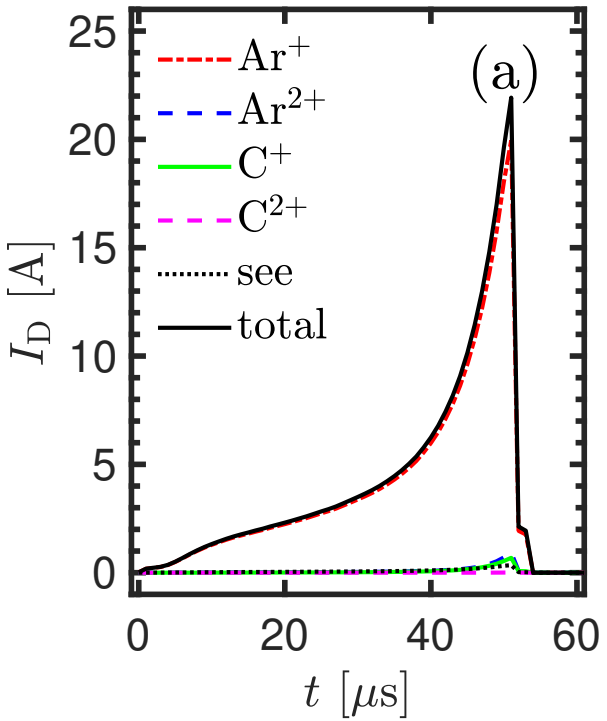

Based on Eliasson et al. (2021) PSST **30** 115017

Recycling in HiPIMS discharges

- Recycling loops
- Discharge with Al or Cu target – SS recycling dominates
  - high self sputter yield
- Reactive discharge with graphite or TiO_2 target – working gas recycling dominates
  - low self sputter yield

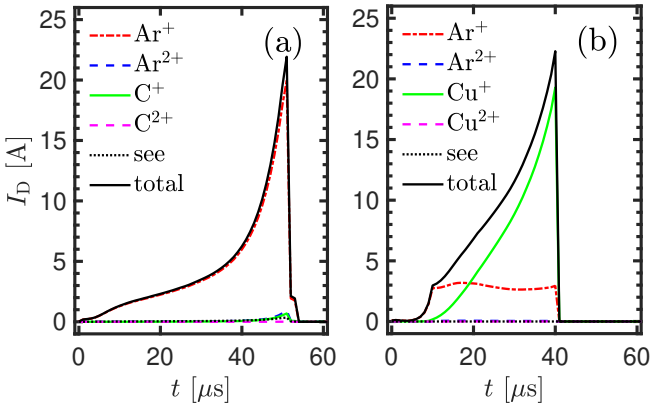

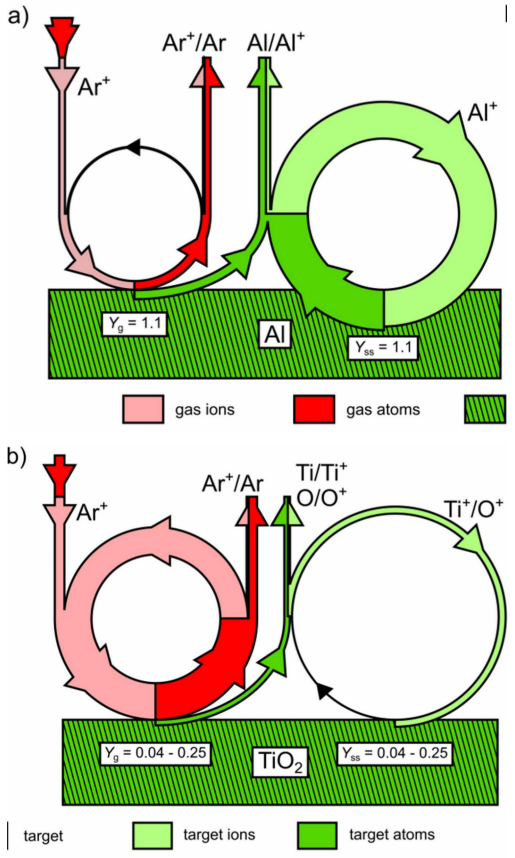

From Brenning et al. (2017) PSST **26** 125003

Recycling in HiPIMS discharges

- What determines the back-attraction probability ?
- How can one influence the back-attraction probability ?
- The back-attraction probability $\beta_{\mathrm{t,pulse}}$, determined by IRM, versus the self-sputter yield for various target materials
- The data indicate that the back-attraction probability decreases roughly linearly with increased self-sputter yield

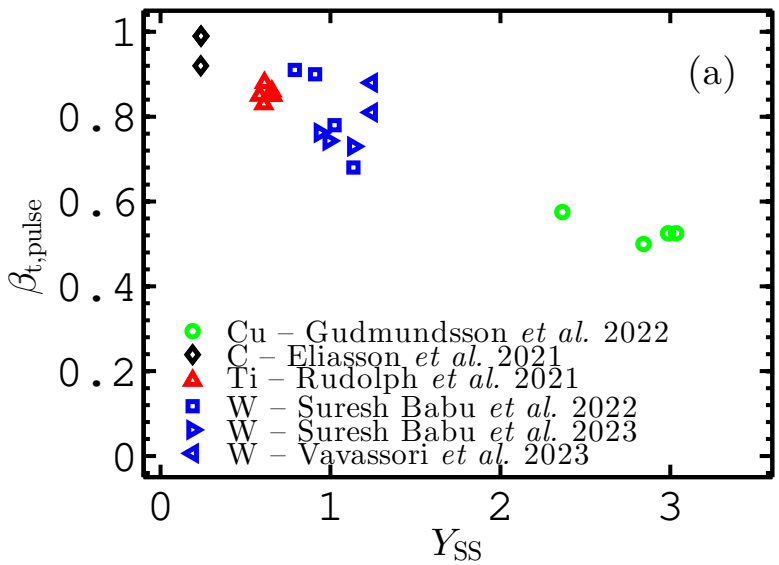

Summary

Summary

- Ohmic heating of the electrons can play a significant role in both dc magnetron sputtering discharge and in particular HiPIMS
- There is an inescapable conflict between the goals of higher deposition rate and higher fraction of ionized species in the sputtered material flux
- In HiPIMS discharge operation there is always recycling:
  - For high currents the discharge with Al or Cu target develops almost pure **self-sputter recycling**, while the discharge with Ti target exhibits close to a 50/50 combination of **self-sputter recycling** and **working gas-recycling**
  - For a poisoned Ti, or a graphite target the sputter yield is low and **working gas-recycling** necessary at high currents

Thank you for your attention

- The work is in collaboration with
  - Swetha Surseh Babu, Ph.D. student, University of Iceland
  - Kateryna Barynova, Ph.D. student, University of Iceland
  - Joel Fischer, Ph.D. student, Linköping University
  - Prof. Daniel Lundin, Linköping University, Sweden
  - Prof. Nils Brenning, KTH Royal Institute of Technology, Stockholm, Sweden
  - Dr. Michael A. Raadu, KTH Royal Institute of Technology, Stockholm, Sweden
  - Dr. Martin Rudolph, Leibniz Institute of Surface Engineering (IOM), Leipzig, Germany
  - Prof. Tiberu Minea, Université Paris-Sud, Orsay, France
  - Dr. Hamidreza Hajihoseini, now at University of Twente, The Netherlands

The slides can be downloaded at

`http://langmuir.raunvis.hi.is/~tumi/ranns.html`

Further reading

- J. T. Gudmundsson, Physics and technology of magnetron sputtering discharges, Plasma Sources Science and Technology, **29**(11) (2020) 113001
- J. T. Gudmundsson, André Anders, and Achim von Keudell, Foundations of physical vapor deposition with plasma assistance, Plasma Sources Science and Technology, **31**(8) (2022) 083001
- Daniel Lundin, Tiberiu Minea and Jon Tomas Gudmundsson (eds.), High Power Impulse Magnetron Sputtering: Fundamentals, Technologies, Challenges and Applications, Elsevier, 2020


Topical Review

Physics and technology of magnetron sputtering discharges

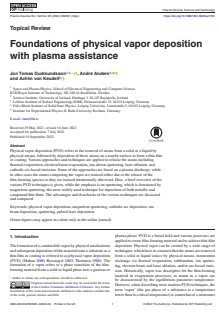
Topical Review

Foundations of physical vapor deposition with plasma assistance

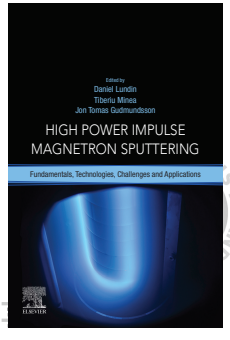

References

Alami, J., P. O. A. Petersson, D. Music, J. T. Gudmundsson, J. Bohlmark, and U. Helmersson (2005). Ion-assisted physical vapor deposition for enhanced film deposition on non-flat surfaces. *Journal of Vacuum Science and Technology A 23*(2), 278–280.

Anders, A., J. Andersson, and A. Ehiasarian (2007). High power impulse magnetron sputtering: Current-voltage-time characteristics indicate the onset of sustained self-sputtering. *Journal of Applied Physics 102*(11), 113303.

Anders, A., J. Čapek, M. Hála, and L. Martinu (2012). The 'recycling trap': a generalized explanation of discharge runaway in high-power impulse magnetron sputtering. *Journal of Physics D: Applied Physics 45*(1), 012003.

Brenning, N., A. Butler, H. Hajihoseini, M. Rudolph, M. A. Raadu, J. T. Gudmundsson, T. Minea, and D. Lundin (2020). Optimization of HiPIMS discharges: The selection of pulse power, pulse length, gas pressure, and magnetic field strength. *Journal of Vacuum Science and Technology A 38*(3), 033008.

Brenning, N., J. T. Gudmundsson, D. Lundin, T. Minea, M. A. Raadu, and U. Helmersson (2016). The role of Ohmic heating in dc magnetron sputtering. *Plasma Sources Science and Technology 25*(6), 065024.

Brenning, N., J. T. Gudmundsson, M. A. Raadu, T. J. Petty, T. Minea, and D. Lundin (2017). A unified treatment of self-sputtering, process gas recycling, and runaway for high power impulse sputtering magnetrons. *Plasma Sources Science and Technology 26*(12), 125003.

Depla, D., S. Mahieu, and R. De Gryse (2009). Magnetron sputter deposition: Linking discharge voltage with target properties. *Thin Solid Films 517*(9), 2825–2839.

Eliasson, H., M. Rudolph, N. Brenning, H. Hajihoseini, M. Zanáška, M. J. Adriaans, M. A. Raadu, T. M. Minea, J. T. Gudmundsson, and D. Lundin (2021). Modeling of high power impulse magnetron sputtering discharges with graphite target. *Plasma Sources Science and Technology 30*(11), 115017.

Gudmundsson, J. T. (2020). Physics and technology of magnetron sputtering discharges. *Plasma Sources Science and Technology 29*(11), 113001.

Gudmundsson, J. T., A. Anders, and A. von Keudell (2022). Foundations of physical vapor deposition with plasma assistance. *Plasma Sources Science and Technology 31*(8), 083001.

Gudmundsson, J. T. (2008). Ionized physical vapor deposition (IPVD): Magnetron sputtering discharges. *Journal of Physics: Conference Series 100*, 082002.

Gudmundsson, J. T., N. Brenning, D. Lundin, and U. Helmersson (2012). The high power impulse magnetron sputtering discharge. *Journal of Vacuum Science and Technology A 30*(3), 030801.

References

Gudmundsson, J. T., J. Fisher, B. P. Hinriksson, M. Rudolph, and D. Lundin (2022). Ionization region model of a high power impulse magnetron sputtering discharge of copper. *Surface and Coatings Technology 442*, 128189.

Gudmundsson, J. T. and A. Hecimovic (2017). Foundations of dc plasma sources. *Plasma Sources Science and Technology 26*(12), 123001.

Gudmundsson, J. T. and D. Lundin (2020). Introduction to magnetron sputtering. In D. Lundin, T. Minea, and J. T. Gudmundsson (Eds.), *High Power Impulse Magnetron Sputtering: Fundamentals, Technologies, Challenges and Applications*, pp. 1–48. Amsterdam, The Netherlands: Elsevier.

Gudmundsson, J. T., D. Lundin, N. Brenning, M. A. Raadu, C. Huo, and T. M. Minea (2016). An ionization region model of the reactive Ar/O_2 high power impulse magnetron sputtering discharge. *Plasma Sources Science and Technology 25*(6), 065004.

Hajihoseini, H., M. Čada, Z. Hubička, S. Ünaldi, M. A. Raadu, N. Brenning, J. T. Gudmundsson, and D. Lundin (2019). The effect of magnetic field strength and geometry on the deposition rate and ionized flux fraction in the HiPIMS discharge. *Plasma 2*(2), 201–221.

Huo, C., D. Lundin, J. T. Gudmundsson, M. A. Raadu, J. W. Bradley, and N. Brenning (2017). Particle-balance models for pulsed sputtering magnetrons. *Journal of Physics D: Applied Physics 50*(35), 354003.

Huo, C., D. Lundin, M. A. Raadu, A. Anders, J. T. Gudmundsson, and N. Brenning (2014). On the road to self-sputtering in high power impulse magnetron sputtering: particle balance and discharge characteristics. *Plasma Sources Science and Technology 23*(2), 025017.

Kateb, M., H. Hajihoseini, J. T. Gudmundsson, and S. Ingvarsson (2019). Role of ionization fraction on the surface roughness, density, and interface mixing of the films deposited by thermal evaporation, dc magnetron sputtering, and HiPIMS: An atomistic simulation. *Journal of Vacuum Science and Technology A 37*(3), 031306.

Kubart, T., M. Čada, D. Lundin, and Z. Hubička (2014). Investigation of ionized metal flux fraction in HiPIMS discharges with Ti and Ni targets. *Surface and Coatings Technology 238*, 152–157.

Magnus, F., A. S. Ingason, S. Olafsson, and J. T. Gudmundsson (2012). Nucleation and resistivity of ultrathin TiN films grown by high power impulse magnetron sputtering. *IEEE Electron Device Letters 33*(7), 1045 – 1047.

Raadu, M. A., I. Axnäs, J. T. Gudmundsson, C. Huo, and N. Brenning (2011). An ionization region model for high power impulse magnetron sputtering discharges. *Plasma Sources Science and Technology 20*(6), 065007.

References

Rudolph, M., N. Brenning, H. Hajihoseini, M. A. Raadu, T. M. Minea, A. Anders, D. Lundin, and J. T. Gudmundsson (2022). Influence of the magnetic field on the discharge physics of a high power impulse magnetron sputtering discharge. *Journal of Physics D: Applied Physics 55*(1), 015202.

Rudolph, M., N. Brenning, M. A. Raadu, H. Hajihoseini, J. T. Gudmundsson, A. Anders, and D. Lundin (2020). Optimizing the deposition rate and ionized flux fraction by tuning the pulse length in high power impulse magnetron sputtering. *Plasma Sources Science and Technology 29*(5), 05LT01.

Rudolph, M., H. Hajihoseini, M. A. Raadu, J. T. Gudmundsson, N. Brenning, T. M. Minea, A. Anders, and D. Lundin (2021). On how to measure the probabilities of target atom ionization and target ion back-attraction in high-power impulse magnetron sputtering. *Journal of Applied Physics 129*(3), 033303.

Rudolph, M., A. Revel, D. Lundin, H. Hajihoseini, N. Brenning, M. A. Raadu, A. Anders, T. M. Minea, and J. T. Gudmundsson (2021). On the electron energy distribution function in the high power impulse magnetron sputtering discharge. *Plasma Sources Science and Technology 30*(4), 045011.

Samuelsson, M., D. Lundin, J. Jensen, M. A. Raadu, J. T. Gudmundsson, and U. Helmersson (2010). On the film density using high power impulse magnetron sputtering. *Surface and Coatings Technology 202*(2), 591–596.

Shimizu, T., M. Zanáška, R. P. Villoan, N. Brenning, U. Helmersson, and D. Lundin (2021). Experimental verification of deposition rate increase, with maintained high ionized flux fraction, by shortening the HiPIMS pulse. *Plasma Sources Science and Technology 30*(4), 045006.

Suresh Babu, S., M. Rudolph, D. Lundin, T. Shimizu, J. Fischer, M. A. Raadu, N. Brenning, and J. T. Gudmundsson (2022). Ionization region model of a high power impulse magnetron sputtering of tungsten. *Plasma Sources Science and Technology 31*(6), 065009.

Suresh Babu, S., M. Rudolph, P. J. Ryan, J. Fischer, D. Lundin, J. W. Bradley, , and J. T. Gudmundsson (2023). High power impulse magnetron sputtering of tungsten: A comparison of experimental and modelling results. *Plasma Sources Science and Technology*, accepted for publication.

Thornton, J. A. (1978). Magnetron sputtering: basic physics and application to cylindrical magnetrons. *Journal of Vacuum Science and Technology 15*(2), 171–177.

Vavassori, D., F. Mirani, F. Gatti, D. Dellasega, and M. Passoni (2023). Role of magnetic field and bias configuration on HiPIMS deposition of W films. *Surface and Coatings Technology 458*, 129343.